WIDE AREA MONITORING AND PROTECTION

A DISSERTATION

Submitted in partial fulfillment of the
requirements for the award of the degree
of
MASTER OF TECHNOLOGY
in
ELECTRICAL ENGINEERING
(With specialization in Power System Engineering)

By

SIDHARTH CHANDAK

DEPARTMENT OF ELECTRICAL ENGINEERING
INDIAN INSTITUTE OF TECHNOLOGY ROORKEE
ROORKEE - 247 667 (INDIA)
MAY, 2016

CANDIDATE'S DECLARATION

I hereby declare that this thesis report entitled **WIDE AREA MONITORING AND PROTECTION**, submitted to the Department of Electrical Engineering, Indian Institute of Technology, Roorkee, India, in partial fulfillment of the requirements for the award of the Degree of Master of Technology in Electrical Engineering with specialization in Power System Engineering is an authentic record of the work carried out by me during the period June 2015 through May 2016, under the supervision of **Dr. Premalata Jena, Department of Electrical Engineering, Indian Institute of Technology, Roorkee.** The matter presented in this thesis report has not been submitted by me for the award of any other degree of this institute or any other institutes.

Date:

Place: Roorkee

SIDHARTH CHANDAK

CERTIFICATE

This is to certify that the above statement made by the candidate is true to the best of my knowledge and belief.

Dr. PREMALATA JENA
Assistant Professor
Department of Electrical Engineering
Indian Institute of Technology Roorkee

Acknowledgements

I would like to express my deep sense of gratitude and sincere thanks to my guide **Dr. Premalata Jena**, Department of Electrical Engineering, Indian Institute of Technology Roorkee, for being helpful and a great source of inspiration. Her keen interest and constant encouragement gave me the confidence to complete my work. I wish to extend my sincere thanks for her excellent guidance and suggestions for the successful completion of my work.

My heartfelt gratitude and indebtedness goes to all the faculty members of Power System Engineering who, with their encouraging and caring words, constructive criticism and suggestions have contributed directly or indirectly in a significant way towards completion of this dissertation.

I would like to thank my parents, god and all my well-wishers who in any manner directly or indirectly have supported and helped me in any part of this work that I have come up in due time.

SIDHARTH CHANDAK

ABSTRACT

Smart grid technology requires intelligent and efficient monitoring of power system network in control centers to prevent unwanted power system blackouts. With recent technological developments, it is now feasible to monitor the health of power system in real time by using wide-area measurement system (WAMS) having phasor measurement units (PMUs). PMUs are considered as an integral and important component in the smart grid era. PMU devices have the ability to provide data measurement at a very fast rate and it can also accurately time synchronize the phasor measurements of the system to a common time reference using GPS signal. This work utilizes PMU data for wide-area backup protection(WABP). Different features using positive and negative-sequence components have been studied and integrated using fuzzy logic to distinguish faults from other power system disturbances more accurately and reliably. The performance of this new protection scheme is evaluated for different types of faults on a modified 400 kV WSCC-9 bus network simulated through EMTDC/PSCAD software. Programming for implementation of proposed algorithm is done in MATLAB environment. Crucial issues such as current inversion, voltage inversion and load encroachment are also addressed.
It is difficult to identify fault inception during power swing condition. Conventional fault detection methods for normal operation of power system finds limitation during power swing condition. A faulted section identification technique during power swing using WAMS has also been presented in this work.

Contents

List of Figures

Abbreviations

SCADA	**S**upervisory **C**ontrol **A**nd **D**ata **A**cquisition
PMU	**P**hasor **M**easurement **U**nit
WAMS	**W**ide **A**rea **M**easurement **S**ystem
WABP	**W**ide **A**rea **B**ackup **P**rotection
PDC	**P**hasor **D**ata **C**oncentrator
UTC	**C**oordinated **U**niversal **T**ime
GPS	**G**lobal **P**ositioning **S**ystem
PPS	**P**ulse **P**er **S**econd
ROCOF	**R**ate **O**f **C**hange **O**f **F**requency
FBI	**F**aulted **B**us **I**dentification
FLI	**F**aulted **L**ine **I**dentification
DFT	**D**iscrete **F**ourier **T**ransform
WSCC	**W**estern **S**ystem **C**oordinating **C**ouncil
FLS	**F**uzzy **L**ogic **S**ystem

Chapter 1

Introduction

Protection Relays are used in power system with the objective to monitor the operating conditions of power system continuously and promptly identify and isolate the faulted section in the system and thereby assuring uninterrupted operation of healthy section. When primary protection fails to clear the fault, then backup protection scheme helps in removing the faulted section from the system. Generally, three step distance protection schemes are used for primary and backup protection of transmission lines.

With ever growing demand for energy, development of interconnected grids and increasing penetration of renewable energy sources has increased the complexity of power system. Analysis of some of the major power system blackout across the globe have revealed that these blackouts were triggered due to mal-operation of back-up protection under stressed and overload conditions [1]. The reason for mal-operation of relay is that its operation is based on the measurement of local quantities and does not take into consideration the information available at remote parts of the system.

1.1 Motivation

For avoiding these blackouts it is necessary to have better system monitoring and protection techniques. Traditionally SCADA system are used for grid monitoring. In SCADA system, measurements are received from meters, transducers, protective relays and RTUs. SCADA system refreshes periodically after 2-10 seconds [3]. Measuring

instruments in SCADA system use local clocks for time stamping their measurements. It is difficult to compare measurements from two different devices because of inconsistency of local clocks. Stability of power system can be easily determined from voltage and current phase angles. But it is difficult to compare the phase angles in SCADA system because of inaccurate time stamping. So, the Dynamic characteristics of the power system can not be monitored by SCADA.

A detailed study of existing conventional backup protection reveals following major drawbacks [4]-

1. There is no coordination among backup protection devices, especially with those in neighborhood of one another. Thus, sometimes mal-operation of backup protection leads to removal of healthy section of power system.

2. Back-up protection does not take into account the impact of power flow transfer because they take decision based on local information.

3. As the complexity of power system is increasing it is becoming more difficult to coordinate Backup protection with primary protection. In some cases, coordination time delay exceeds the threshold value and violates the system security and reliability.

With recent technological advancements, requirements of better system monitoring and protection can be achieved by phasor measurement unit (PMU) based wide-area measurement system (WAMS) [2]. It is an interesting and trending area of research among power engineers. Time delays involved in communication of data in WAMS makes it a lucrative method for supplementing existing backup protection techniques. Wide-area back-up protection (WABP) algorithms uses PMU data for developing robust and efficient protection schemes.

1.2 Literature Review

Various protection schemes based on WAMS have been reported in the literature. In [5], bus in the proximity of the fault is identified by comparing positive-sequence voltage magnitude of all the buses in the system and then positive-sequence current phase angle difference is used to determine the faulted line connected to that bus.

In [6], residual vector of synchrophasor state estimator (SynSE) is utilized to supplement the zone-3 protection to further improve the security of the system.

A WABP method based on steady state differential current component is used in [7] to indicate the faulted line inside a protection correlation region (PCR). These PCR are formed based on PMU placement and network topology.

Fault component voltage distribution based algorithm is used in [8] for WABP. Fault component current and voltage measured at one end of the line are used in estimation of fault voltage at the other end of the transmission line. Ratio of measured value to the estimated value is used for identification of faulted line.

Sum of positive and zero-sequence current is utilized in [9] for determining the faulted backup protection zone. These backup protection zones are formed depending on network configuration and PMU positions. Current and voltage of the faulted backup protection zone are then used by least square based method to determine the faulted section.

In [10], an artificial intelligence based WABP technique is proposed to prevent cascaded outages in power system and minimize the impact of faults.

A non-intrutive agent based relay supervised distance protection method is discussed in [11]. Transmission lines have relays for protection and each relay is assigned with a master and a slave agent. These agents communicate with each other to take final decision as fault or non fault condition.

A wide area differential backup protection using graph theory is presented in [12] for smart grid application. Different dynamic online protection zones are formed by using graph theory and differential current protection is used in protected zones to identify the faulted section.

In [13], Wide area protection method based on fusion of information from multiple sources is used for identification of faulted element. A grid topology based fault identification encoding technique is proposed. Fitness function and state expectation function are determined based on breaker status and information of traditional protection relays. Fault probability is estimated based on fitness of protected element.

To meet the growing power demand, difficulty in erecting new transmission lines, regulatory regulations and several other technical benefits has encouraged the use of series compensation in long transmission lines. However, inclusion of series capacitor and

its over voltage protection device (air gap and/or metal-oxide varistor (MOV)) creates trouble for distance relaying based protection. Various issues associated with relays have been discussed in [22]-[25]. Some typical issues include voltage/current inversion, sub-harmonic oscillations etc. Various WABP techniques present in the literature have not been tested for transmission lines with series compensated and may not perform adequately for these transmission lines.

1.3 Thesis Organization

The remaining of this thesis comprehends four chapters. In Chapter 2, WAMS basic architecture, important components and applications have been discusses. In chapter 3, a WABP scheme for series compensated line has been studied and its results are discussed. In chapter 4, a new method for faulted element identification during power swing has been discussed along with results for different types of faults and condition. In chapter 5, fuzzy logic based data integration technique for protection of series compensated line has been discussed along with its performance for different faults and conditions. In chapter 6, conclusion and future work has been reported.

Chapter 2

Wide Area Measurement System

WAMS can measure power system phase angles accurately and synchronously. This is one of the main advantage of WAMS over SCADA systems which cannot measure these phase angles directly. WAMS provides dynamic behavior of power system to the operator as reporting rates of PMU are much faster than those of SCADA system. Presently, PMUs with measuring rates of upto 120 frames/s are available in the commercial markets.

PMU was invented by Dr. Arun G. Phadke and Dr. James S. Thorp at Virginia Tech in 1988 and the first PMU (model-1690) was developed by Macrodyne in 1992 [15]. This technology has come in limelight in recent days and is gaining world wide acceptance. Many large scale PMU deployment projects are already completed/going on in asia, europe and america. In India, PMU based Unified Real-time Dynamic State Measurements (URTDSM) has been proposed for grid monitoring. Approximately 1669 PMUs will be installed in two phases.

2.1 Main Components in WAMS

There are three main components in WAMS system. These components are-

- Phasor Measurement Unit (PMU)
- Phasor Data Concentrator (PDC)

- Communication network

WAMS architecture used by utilities all over the world vary depending on their requirements and economy. In a most common architecture, PMUs send their measurements from different substations in the network to control centers as shown in Figure 2.1.

PMUs installed in the substation computes 3-phase and/or sequence components syn-

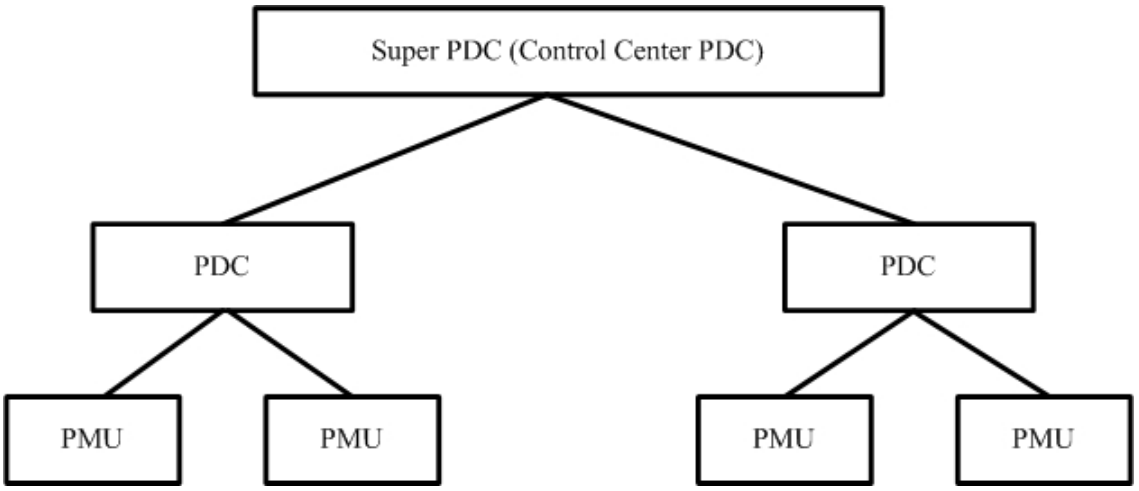

FIGURE 2.1: Basic architecture of WAMS

chrophasors. These computed synchrophasors are sent to phasor data concentrators (PDCs). Synchrophasors can also be stored locally in the PMU. A PDC receive synchrophasors from PMUs and arrange them according to their time tags and then send it to the PDC in control center. In the control center, synchrophasors are utilized for different applications.

2.1.1 Phasor Measurement Unit

The nature of current and voltage waveform in power system network is sinusoidal. A sinusoidal signal can be represented in time domain as -

$$x(t) = X_m cos(2\pi ft + \phi) \tag{2.1}$$

where, X_m is the magnitude, ϕ denotes the phase angle, t denotes time and f represents the frequency of the sinusoid. In complex plane, sinusoidal signal can be represented by phasors. The term 'phasors' was first coined by Charles Proteus Steinmetz in 1893.

Sinusoidal signal of (2.1) can be written in phasor domain as -

$$X = \frac{X_m}{\sqrt{2}}\angle\phi = X_{re} + jX_{img} \tag{2.2}$$

or

$$X = X_{re} + jX_{img} \tag{2.3}$$

where X_{re} is the real component and X_{img} is the imaginary component of the phasor. Equation (2.3) is independent of frequency, hence phasors are defined at a particular frequency only.

According to IEEE standards, Synchrophasors are described as phasors computed from samples of data utilizing a standard time signal as the reference for measurements. In simple terms, these are phasors calculated with a common and an accurate time source as reference. PMU uses UTC (Coordinated Universal Time) for time synchronization. UTC is one of the widely accepted international time standard. PMU uses Global Positioning System (GPS) system for obtaining UTC time.

GPS system consist of a group of satellites which transmits signals to the user. GPS system was built by U.S. Department of Defense (DoD) with the main objective of providing precise location and time information. Presently GPS system consist of 31 operational satellites. First satellite for this project was launched in 1978 [16]. Minimum 24 operational satellites are required for proper functioning of GPS system, extra satellites helps in enhancing the performance of GPS. Each GPS satellite is orbiting earth at an altitude of 20,180 km approximately. Six different orbital planes displaced 60° from each other are used by GPS satellite for revolving around the earth. These satellites are positioned around the earth in such a way that any location on earth has access to atleast four satellites. The GPS satellite has atomic clocks installed in them, these clocks can be updated from a ground station. GPS receiver are used to receive signals transmitted by by GPS satellite. However, slowing down of earth's rotation is not reflected in GPS time signal. Necessary correction in GPS time to consider the effect of leap-second is done by GPS receiver. Corrections are made before providing the UTC time. Pulse-per-second (pps) signals are send from GPS satellite to GPS receiver [16]. The received pps signal of a GPS receiver is coincident with those received by other GPS receivers.

Different vendors provide different block diagram representation of PMUs. A general schematic is as given in Figure 2.2. Time synchronization to the measurements of PMU is provided by pps signal of GPS.

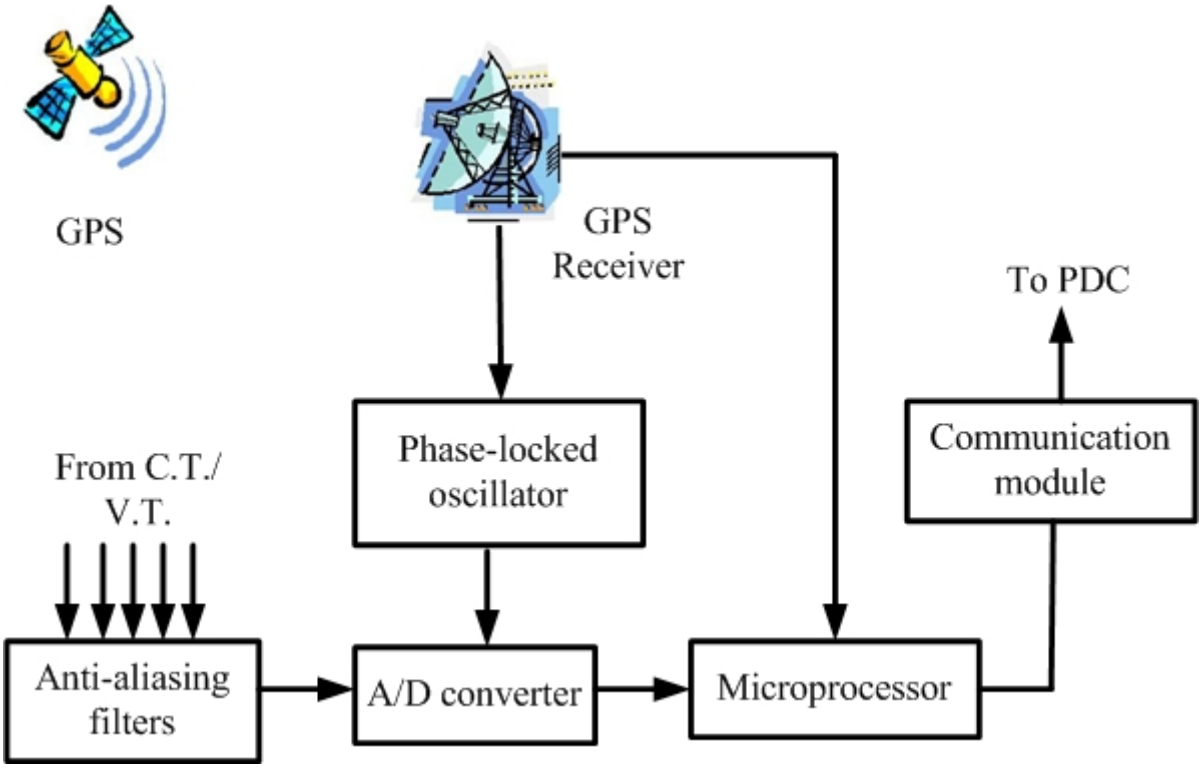

FIGURE 2.2: Block diagram of a PMU

Analog inputs such as phase voltages and currents information are obtained by PMU. These input analog signals are received from the secondary of current transformer and voltage transformer. To prevent aliasing error, these inputs are passed through a anti-aliasing filter. Signals having frequency less that half the sampling frequency are removed at the output of anti-aliasing filter. Frequency dependent phase delays are introduced by anti-aliasing fliter, these delays have to be taken care of before synchrophasors are produced. To block the transients generated by switching operatios, PMU is also provided with surge suppressing filter. Analog to digital (A/D) converters are used to convert analog input signals to digital values. Generally 16 bit A/D converter are used in PMU. A/D converter sampling clock is phase locked with 1 pps signal of GPS. Phase locked oscillator uses 1 pps signal to produce a sequence of high speed timing pulses for A/D sampling [16]. Digital samples are used by microprocessor to compute synchrophasors of phase voltage and current along with positive, negative and zero-sequence components. Other important parameters such as circuit breaker status, frequency, rate of change of frequency (ROCOF) are also computed by the microprocessor [20]. PMU send these

computed values to PDC via some communication channel. PMU reporting rates for 50 Hz system are 10, 25,50 frames/s and for 60 Hz system are 10, 12, 15, 20, 30, 60, 120 frames/s.

2.1.2 Phasor Data Concentrator

A PDC can be operated as a standalone device or it can be integrated into other systems. PDC perform some of the important functions in WAMS technology. These are as follow-

- Data Communication: A PDC has to communicate with PMUs and other PDCs.
- Data Alignment: A PDC receive time stamped measurements from different PMUs. PDC arranges these incoming synchrophasors depending on their time stamp. It waits for data of a particular timestamp from all the input sources and once all the synchrophasors belonging to a specific time tag are received, it puts them in a data packet. These data packets are then send to another PDC or to a specific application.
- Data Validation: PDC perform data validation for data integrity, time quality and other checks to detect and flag any corrupt data before it is send out.
- Reporting Rate Conversion: PDC receives data from different PMUs. These PMUs may have different reporting rates. So, a PDC should be able to convert the reporting rate of incoming synchrophasors.

2.1.3 Communication Network

PMUs are installed in substations which are spread over a wide geographical region and these substation are located at a very long distance from control center where PDC is placed. Communication network becomes an import aspect in implementation of WAMS as synchrophasors measured by PMUs have to be to communicated to PDCs in control center. Power grid monitoring is a real time application. WAMS communication network should have high speed, reliability and security. Most of the power utilities are using dedicated network for WAMS communication because delay in communication effects the performance of synchrophasor based applications. However, communication delays can not be eliminated completely from the system and occurs depending on propagation delay, network bandwidth and various data processing stages such as multiplexing, buffering etc. The amount of data that can be transmitted over a communication

network is directly proportional to the bandwidth of the network. Propagation delay mostly depends on communication medium. Different communication options available for WAMS are as follow-

- Telephone Lines: These are one of the easy to set up and economical data communication option for utilities. Data rates of upto 56 kbps can be achieved by telephone lines.
- Satellites: Low-earth orbiting (LEO) satellites can also be used for WAMS communication. But this type of communication involves large capital investment and has narrow bandwidth.
- Power Lines: Power line communication (PLC) is a technique in which power lines are themselves used for data transfer along with electrical signals. Presently this technology is being considered for WAMS applications as it offers easy access to remote substation but suffers from the drawbacks like signal distortion and attenuation. It uses frequency in the range of 24 kHz to 500 kHz.
- Microwave Links: Microwave links are used as communication medium in situtaions where remote PMUs can not be connected to PDC by a wired connection economically. Multi-path propagation and signal fading are its main drawbacks.
- Fiber Optics Cable: One of the most attractive option for WAMS communication is fiber optics cable based communication network. These can be used for long distance signal transmission without any distortion. It offers large bandwidth in the range of terabytes per second and has low latency.
- Digital Microwave Radio: Digital microwave radio communication is based on line of sight(LOS) and troposphere scattering communication. It can be operated in 2 GHz band or 8 GHz band. It offers bandwidth of upto 34 mbps. But it is suitable only for distances upto 40-70 km depending upon the terrain.

For sending synchrophasor data to PDC, a PMU needs to follow a communication protocol. RS-232 based serial communication was used in early days. Its main drawback is limited maximum data throughput. Now a days internet protocols are being used. Some of the commonly used internet protocols are TCP only, UDP only and TCP/UDP. TCP offers more reliability than UDP protocol but UDP has fewer bandwidth requirements than that of a TCP protocol.

2.2 IEEE Standards

First PMU standard was IEEE standard 1344-1995. This standard mainly discussed PMU interfacing with the system, format for timing input, sample synchronization and format for phasor data output [17]. In 2005, IEEE standard 1344-1995 was replaced by an updated version of standards named as IEEE standard C37.118-2005. The standard C37.118-2005 contained synchrophasor definition, format of message to communicate with a PMU and compliance testing methods. The convept of total vector error (TVE) was also introduced. These standards were specified for steady state operation of power system [18].

In 2011, synchrophasor standard C37.118-2005 was replaced by two new standards. The IEEE standard C.37.118.1-2011 is associated with measurements of PMUs and IEEE standard C.37.118.2-2011 is concerned with communication aspects. Standard C.37.118.1-2011 also include definition of synchrophasors, test procedure and accuracy limits for dynamic operation of power system. It also includes accuracy limits of PMU for frequency ramping, small signal oscillations. step change, power system frequency and ROCOF. Standard C.37.118.2-2011 have standards for message format, message types and message contents for real time communication netween PMUs and PDCs [19]. It describes four types of messages-

1. Data frame
2. Configuration frame
3. Command frame
4. Header frame

Measurements measured by PMU are present in data frames. Machine readable information about data sent by PDC/PMU is contained in configuration frame. Command frame contains appropriate actions to be taken in machine readable format. Human readable information is in header frame.

Untill 2013, there were no IEEE standards to benchmark the performace criteria for PDCs. In 2013, IEEE has released standard C37.244-2013 which contains PDCs testing and functional requirements [21].

2.3 Applications of WAMS

Application of wide area measurement system in the domain of power system is in its early days. Many power system utilities across the world have installed PMUs and PDCs in their network. However, compared to complexity of the present power system network, number of these devices is very less. As this technology becomes more mature, it is believed to be a vital component in power networks of the future. Some of the key applications of WAMS can be easily grouped as follow-

- Backup protection of power system
- Real time monitoring of power system
- Voltage and angular stability analysis
- Advanced control schemes

Chapter 3

Wide Area Backup Protection

A symchrophasor based WABP proposed in [14] has been studied. It uses faulted bus identification (FBI) followed by faulted line identification (FLI) algorithm. It uses two different methods for balanced and unbalanced faults. For balanced faults, FBI is done by using magnitude of positive-sequence voltage and FLI is done by cosine of angle between positive-sequence fault current and positive sequence fault voltage at both terminals of the line. For unbalanced faults, magnitude of negative and zero-sequence bus voltage is used for FBI and cosine of angle between negative-sequence fault current and negative-sequence fault voltage at both terminals of the line are used for faulted line identification. Modified 400 kV WSCC 9 bus system is used for testing the method studied [26]. Availability of the PMUs at each bus of the system is assumed. Full cycle Discrete fourier transform (DFT) method has been used for estimating fundamental frequency sequence components. Phase-a is taken as the reference and sampling frequency of 1 kHz is used. EMTDC/PSCAD has been used for simulating the WSCC-9 bus system. The System data are given in Appendix.

3.1 Proposed Method

3.1.1 Faulted Bus Identification

Whenever a fault appears in a power system, the bus nearest to the fault location is effected the most. Hence, comparison of voltage magnitude of different buses is used for

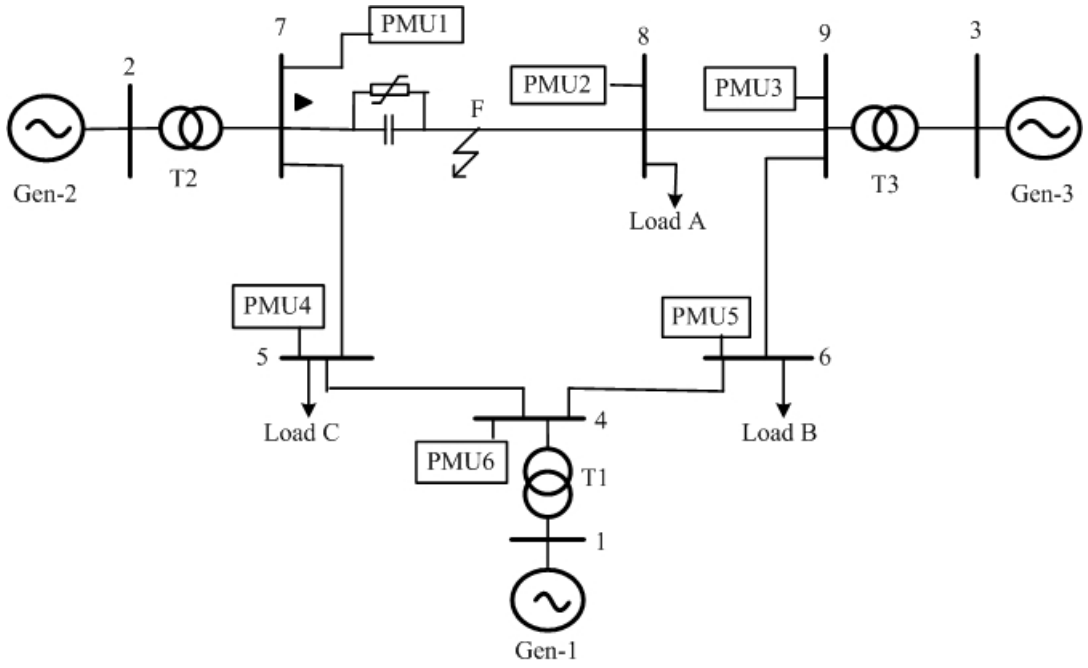

FIGURE 3.1: Modified WSCC 9 bus system single line diagram representation along with PMUs

the task of FBI. For unbalanced faults, negative and zero-sequence components of bus voltage are used [8]. Fault pickup condition is defined as

$$(|\vec{V}_{m2}| \geq K_2 V_N) \cup (|\vec{V}_{m0}| \geq K_0 V_N) \tag{3.1}$$

where $\vec{V}_{m2}$ and $\vec{V}_{m0}$ are m^{th} bus negative and zero sequence voltage components and V_N is the amplitude of rated voltage. K_2 and K_0 are proportionality constants to set the thresholds for negative and zero sequence-components. Values of K_2 and K_0 are set at 0.1. If equation (3.1) is not satisfied then balanced fault condition is checked as

$$(|\vec{V}_{m1}| \leq K_1 V_N) \tag{3.2}$$

where K_1 is the proportionality constant for positive-sequence component of voltage and is set at 0.6 [5]. Ideally, bus with the maximum magnitude of negative or zero-sequence component or with the lowest magnitude of positive-sequence component should be considered as the bus nearest to the fault location. However, to consider the effect of various miscellaneous factors such as measurement error, load demand etc. All the buses which satisfy above criteria are selected and are checked for FLI in a sorted manner from top to bottom till faulted line is identified.

3.1.2 Faulted Line Identification

1. FLI for Unbalanced Fault:

Negative-sequence based quantities are used for identifying unbalanced faults because positive-sequence quantities are affected by unbalanced faults having high fault resistance. The angle (ϕ_2) between neagtive-sequence fault current and fault voltage is utilized in this technique. The values of (ϕ_2) during forward/downstream fault and backward/upstream fault is $-90° < \phi_2 < 0°$ and $90° < \phi_2 < 180°$ respectively [27]. For a series compensated line, above criteria find limitations for conditions of voltage and current inversion.

Voltage inversion occurs when the impedance between fault point and the relay bus is capacitive and total impedance between fault point and source is inductive. Current inversion occurs when relay and source voltages are in phase and there is large capacitance in fault loop such that capacitive reactance is greater than equivalent reactance from source to fault location [28].

To simulate voltage and current inversion for series compensated system. Line 7-8 of

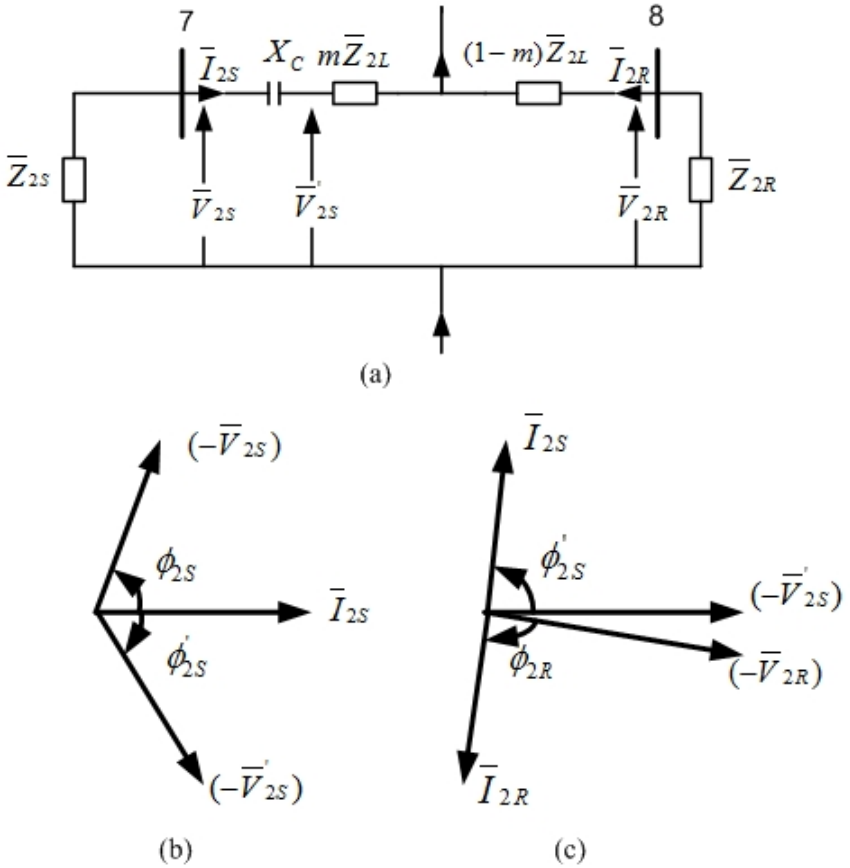

FIGURE 3.2: (a) Diagram of Negative-sequence network for a LG fault at point F. (b) Phasor diagram for voltage inversion. (c) Phasor diagram for current inversion.

Figure 3.1 is provided with 70% series compensation. A single line to ground fault is simulated in phase-a at point F of the line 7-8. Diagram of equivalent negative-sequence network and corresponding phasors are shown in Figure 3.2. For voltage inversion case, voltage $V_{2s}^{'}$ is inverted. Hence, current leads voltage and if relay is polarized with line side voltage then it will be declared as upstream fault even though it is a downstream fault. Similarly current inversion also causing the relay to mal-operate as shown by phasor diagram of Figure 3.2(a) and (b) respectively.

However, from the phasor diagram drawn in Figure 3.2, it can be concluded that $\phi_{2S}^{'}$ varies in the range of $-90°$ to $90°$ for a forward fault at bus 7 with and without current or voltage inversion. For this range of values of $\phi_{2S}^{'}$, $cos(\phi_{2S}^{'})$ is always positive. This feature has been used in FLI for unbalanced fault in a power network without and with series compensation. Let $g_{2S} = cos(\phi_{2S})$, $g_{2S}^{'} = cos(\phi_{2S}^{'})$ and $g_{2R} = cos(\phi_{2R})$, where $\phi_{2S}^{'}$ and ϕ_{2S} represents the phase angle between negative-sequence components of fault current and fault voltage after and before the series capacitor and ϕ_{2R} is the line's other end angle between negative-sequence components of fault current and fault voltage. FLI criteria is defined as

$$g_{2S} > 0 \cap g_{2S}^{'} > 0 \cap g_{2R} > 0 \tag{3.3}$$

2. FLI for Balanced Fault:

For identification of balanced fault , phase angle (ϕ_1) between positive-sequence component of fault current and fault voltage is used. During forward fault,range of ϕ_1 is $-90° < \phi_1 < 0°$ and backward fault's range is $90° < \phi_1 < 180°$ [27]. However, these conditions are not true for the case of current and voltage inversion.

Current and voltage inversion leads to declaration of a forward fault as backward fault by the relay. Consider a 3 ϕ fault on line 7-8 at point F. Equivalent positive sequence impedance diagram of line having series compensation with MOV protection is shown in Figure 3.3. In this figure, $R_C^{'}$-j$X_C^{'}$ represents the equivalent impedance of series capacitor and MOV [29]. Equivalent positive-sequence impedance of the source is given by R_{1S}+jX_{1S} and positive-sequence impedance of the line upto the fault point is given by R_{1L}+jX_{1L}. During voltage inversion, I_{1S} leads V_{1S} as represented in Figure 3.3(c) and angle between them have a sign opposite of that without inversion. Hence, relay at bus 7 will give wrong decision if polarized with bus side voltage. Similarly for the case of current inversion, phasor diagram is as shown in Figure 3.3(d), again relay will give wrong decision. However, from the phasor diagrams of Figure 3.3, it can be concluded that ϕ_{1S} varies in the range of $-90°$ to $90°$ for a forward fault at bus 7 with and without

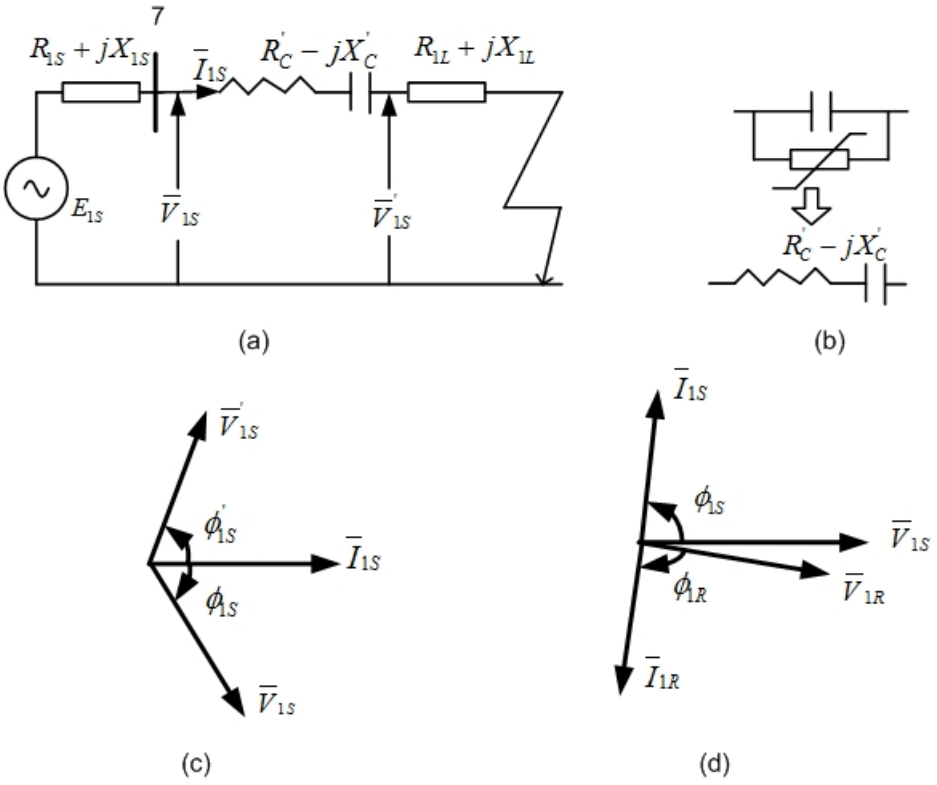

FIGURE 3.3: (a) Diagram of positive-sequence network for a three phase fault at point F. (b) Representation of the series capacitor and MOV by equivalent impedance. (c) Phasor diagram for voltage inversion. (d) Phasor diagram for current inversion.

current/voltage inversion. For this range of values of ϕ_{1S}, $cos(\phi_{1S})$ is always positive. This feature has been used in FLI for balanced fault in a power network without and with series compensation. Let $g_{1S} = cos(\phi_{1S})$, $g_{1S}^{'} = cos(\phi_{1S}^{'})$ and $g_{1R} = cos(\phi_{1R})$, where $\phi_{1S}^{'}$ and ϕ_{1S} represents the phase angle between positive-sequence component of fault current and fault voltage after and before the series capacitor and ϕ_{1R} is the line's other end angle between positive-sequence component of fault current and fault voltage. FLI criteria is defined as

$$g_{1S} > 0 \cap g_{1S}^{'} > 0 \cap g_{1R} > 0 \tag{3.4}$$

Flowchart of the algorithm is shown in Figure 3.4.

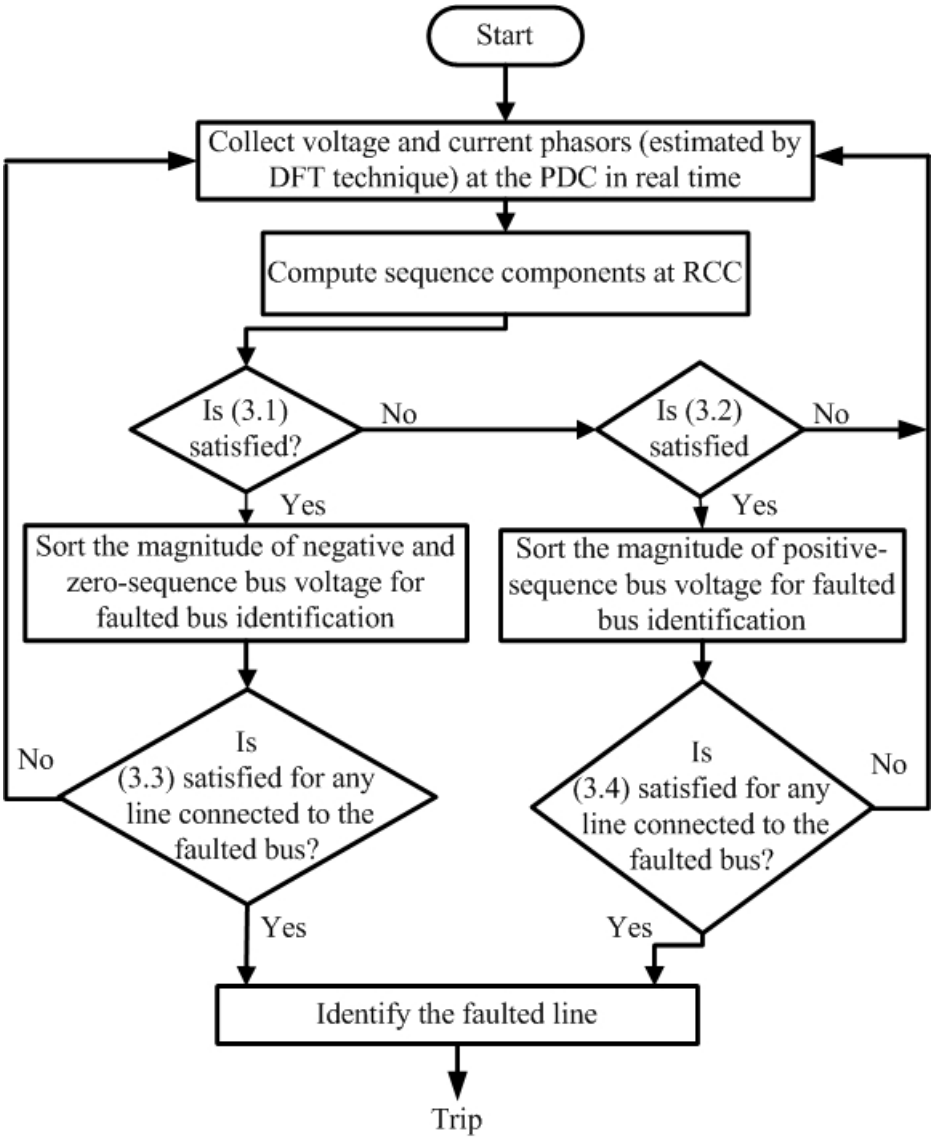

FIGURE 3.4: Flowchart of WABP scheme.

3.2 Results

3.2.1 Results for Current Inversion during Unbalanced Fault

For simulating the condition of current inversion, line 5-7 is removed from the network shown in Figure 3.1 and Gen-2's source impedance is reduced. After these modifications are made in the system, A Lg fault is created in phase-A of line 7-8 at a distance of 30 km from bus 7 with fault resistance of 75 Ω at 1 s. Figure 3.5 shows current and voltage at both terminals of the line 7-8 and it can be inferred from these figures that current and voltage at both terminals of the line are out of phase and in phase respectively. So, current inversion condition is confirmed.

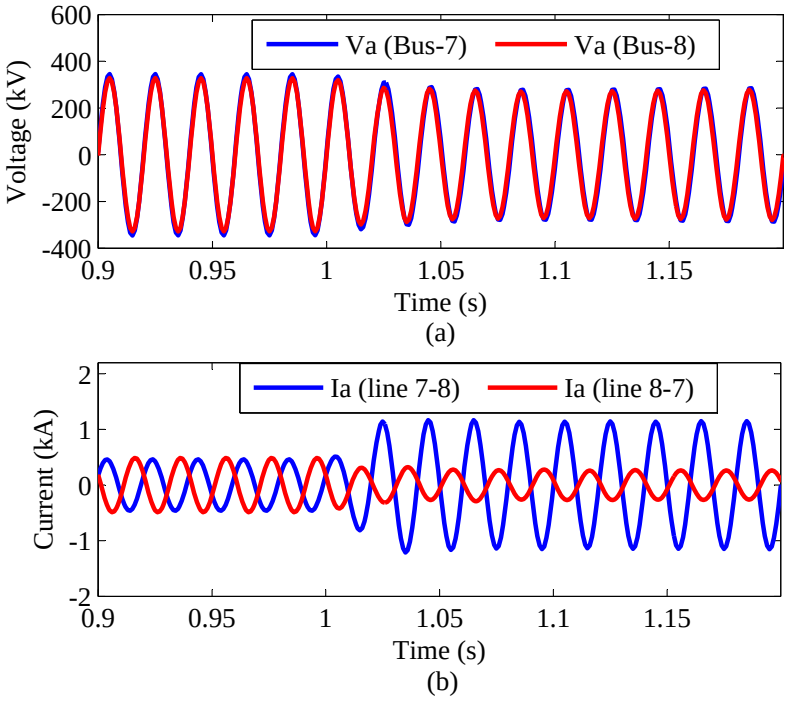

FIGURE 3.5: (a) Voltage and (b) Current of phase-A at both terminals of line 7-8 for an A-g fault.

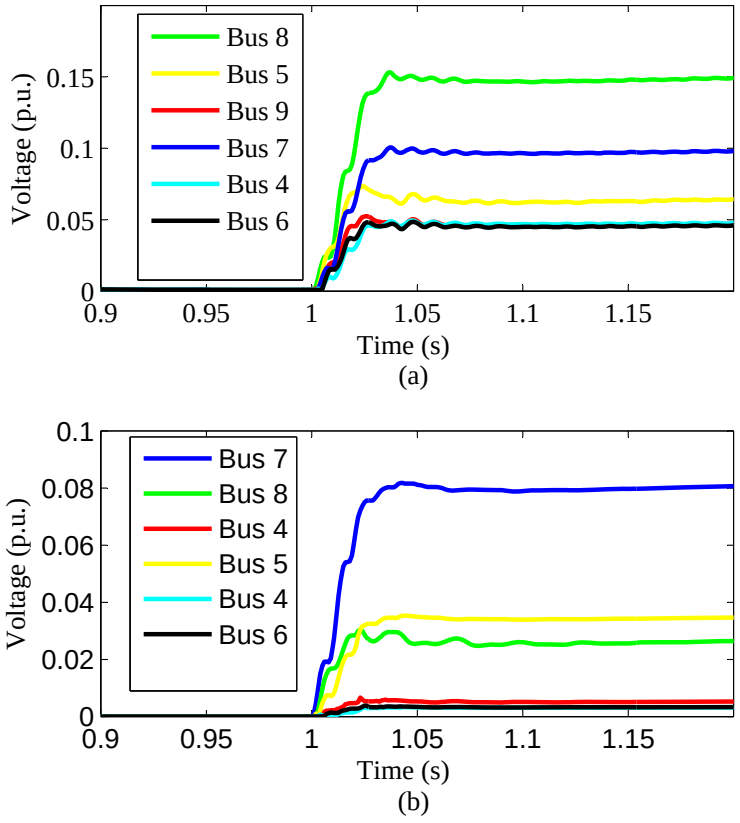

FIGURE 3.6: Magnitude of (a) Negative and (b) Zero sequence voltage.

Negative and zero-sequence voltage magnitude variation is plotted in Figure 3.6. It can be clearly inferred from these figure that bus 8 satisfy the FBI criteria. For FLI, ϕ'_{2S}, ϕ_{2S} and ϕ_{2R} of line 7-8 along with their indices g'_{2S}, g_{2S} and g_{2R} are plotted in Figure 3.7(a) and (c) respectively. ϕ_{2S} and ϕ_{2R} of line 8-9 along with their indices g_{2S} and g_{2R} are shown in Figure 3.7(b) and (d) respectively. As g'_{2S}, g_{2S} and g_{2R} of line 7-8 are all positive, so it is declared as faulted line based on FLI algorithm.

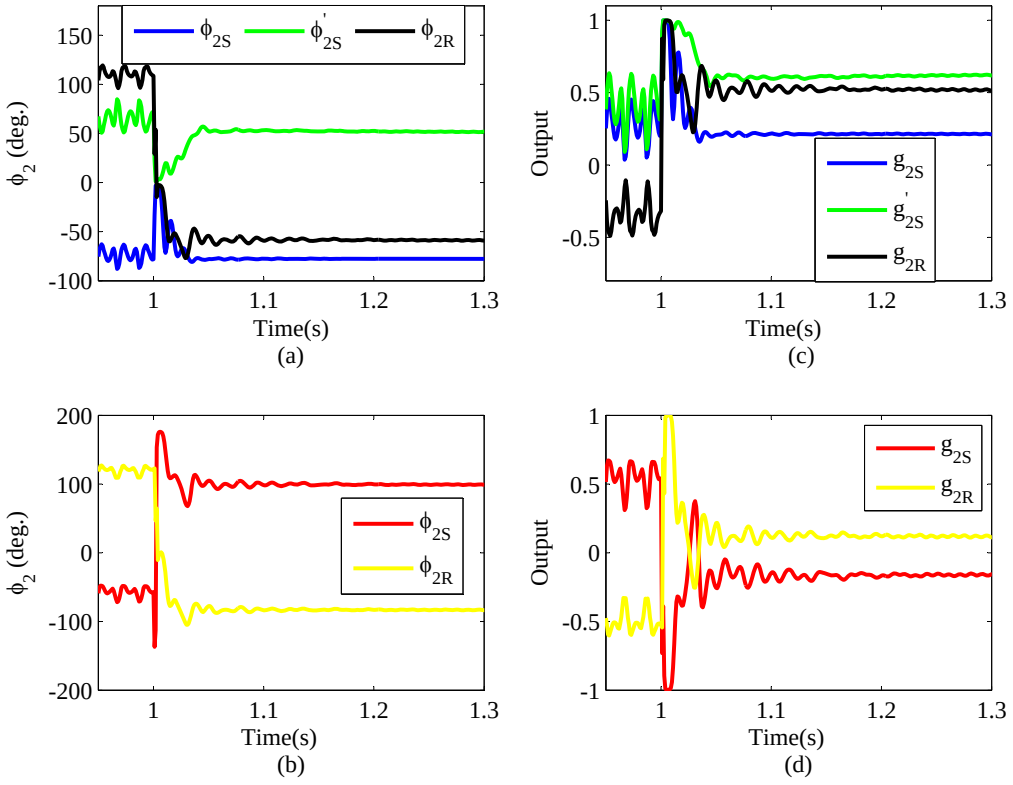

FIGURE 3.7: Performance during current inversion. Angles at both terminals of (a) Line 7-8 and (b) Line 8-9. Output indices of (c) Line 7-8 and (d) Line 8-9.

3.2.2 Results for Voltage Inversion during Balanced Fault

To evaluate the performance of studied technique for voltage inversion, a 3 ϕ fault is simulated in line 7-8 at a distance of 60 km from bus 7 at 1 s. Figure 3.8(b) shows current of phase-a at both ends of the line 7-8 and phase-A voltage after and before the series capacitor is shown in Figure 3.8(a). It can be inferred from these figures that voltage and current are out of phase and in phase respectively. So, voltage inversion condition is confirmed.

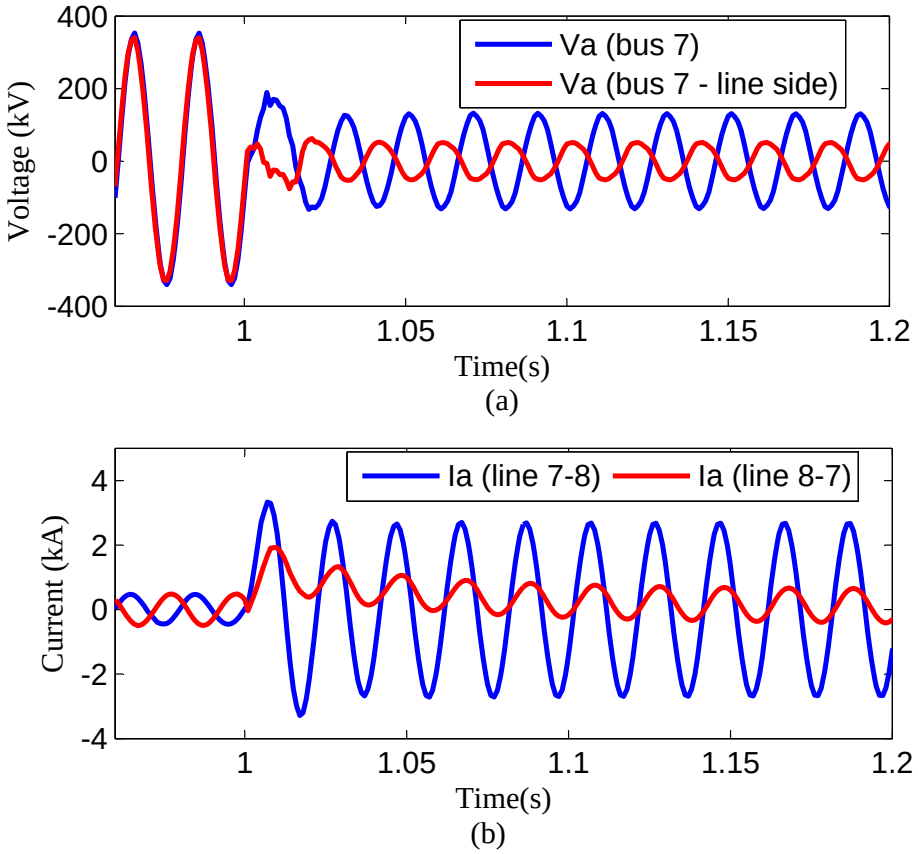

FIGURE 3.8: (a) Voltage of phase-A after and before series capacitor. (b) Current of phase-A at both terminals of line 7-8.

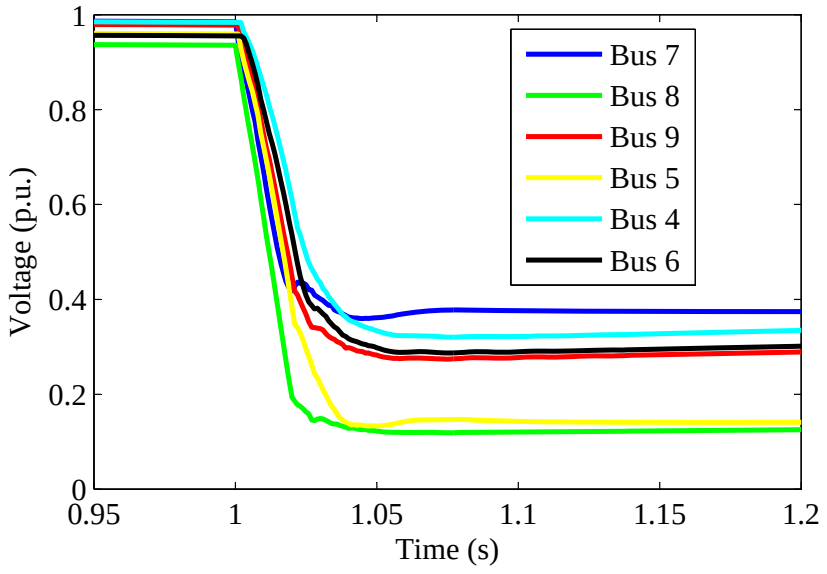

FIGURE 3.9: Magnitude of positive-sequence bus voltages.

Positive-sequence voltage magnitude variation is given in Figure 3.9. It can be clearly inferred from this figure that bus 8 satisfy the FBI criteria. For FLI, ϕ'_{1S}, ϕ_{1S} and ϕ_{1R} of line 7-8 along with their indices g'_{1S}, g_{1S} and g_{1R} are plotted in Figure 3.10(a) and (c)

respectively. ϕ_{1S} and ϕ_{1R} of line 8-9 along with their indices g_{1S} and g_{1R} are shown in Figure 3.10(b) and (d). As g'_{1S}, g_{1S} and g_{1R} of line 7-8 are all positive, so it is declared as faulted line based on FLI algorithm.

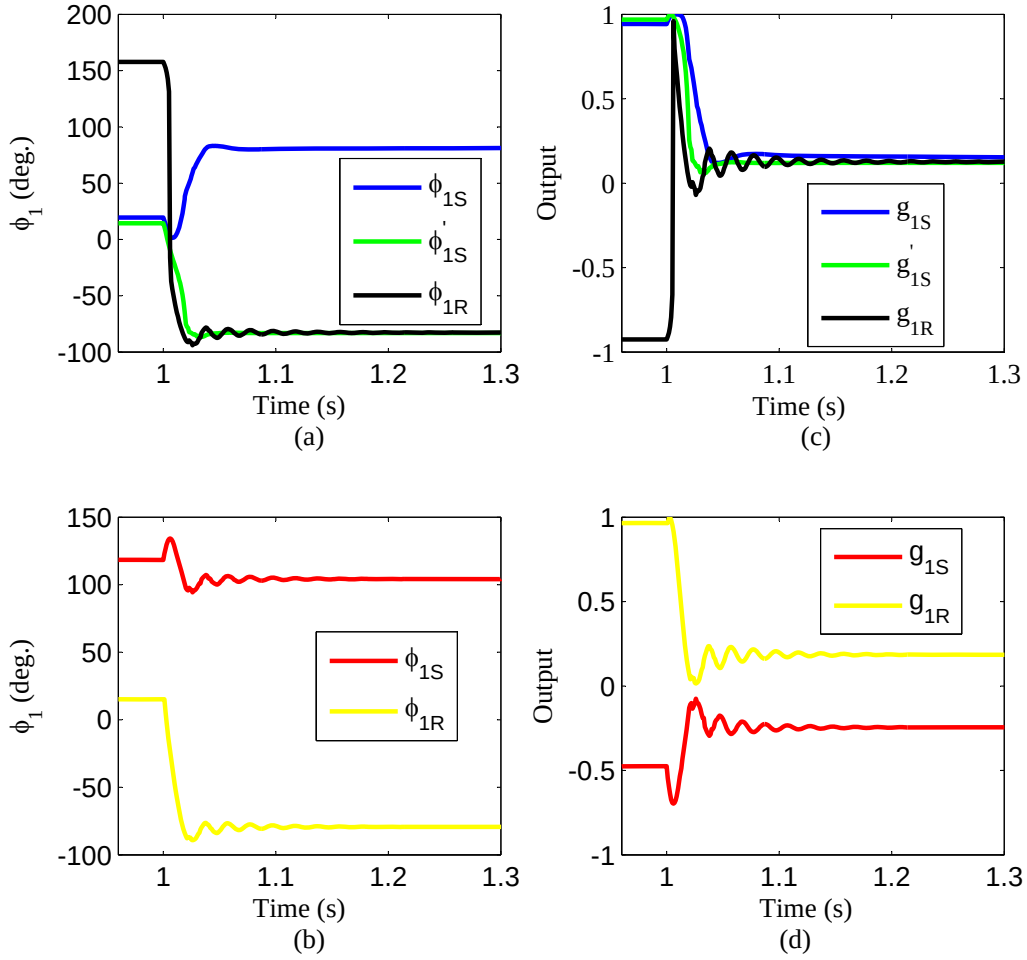

FIGURE 3.10: Performance during voltage inversion. Angles at both terminals of (a) Line 7-8 and (b) Line 8-9. Output indices of (c) Line 7-8 and (d) Line 8-9.

3.2.3 Performance for Load Encroachment

To simulate the condition of load encroachment for zone 3 of relay at bus 7 in Figure 3.1, load at bus 8 is increased slowly so that there is increase in current of line 7-8 but it is kept below the NERC "extreme loading limit". Plot of positive-sequence impedance measured by relay at bus 7 under this condition on R-X plane is shown in Figure 3.11. As measured impedance enters the operating region of zone 3 of the relay,so this would lead to false tripping of line 8-9. Positive-sequence voltage magnitude variation is plotted in Figure 3.12. From this figure it can be inferred that bus 8 voltage satisfy the FBI condition so WABP algorithm will trigger FLI criteria for the lines connected to

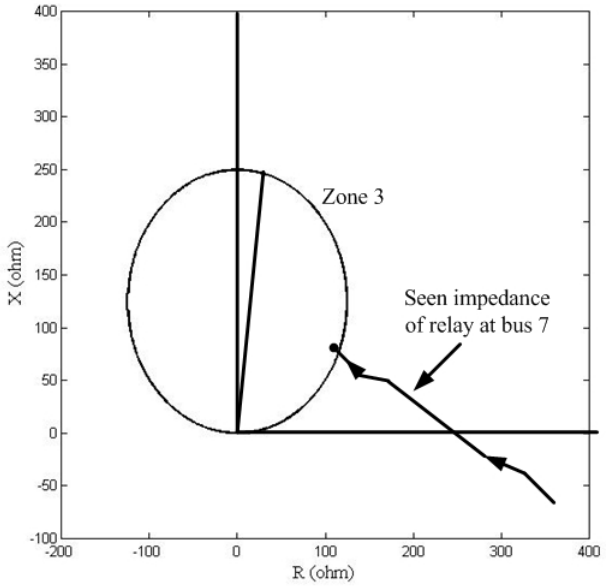

FIGURE 3.11: Trajectory of positive-sequence impedance seen by relay at bus-7 during load encroachment.

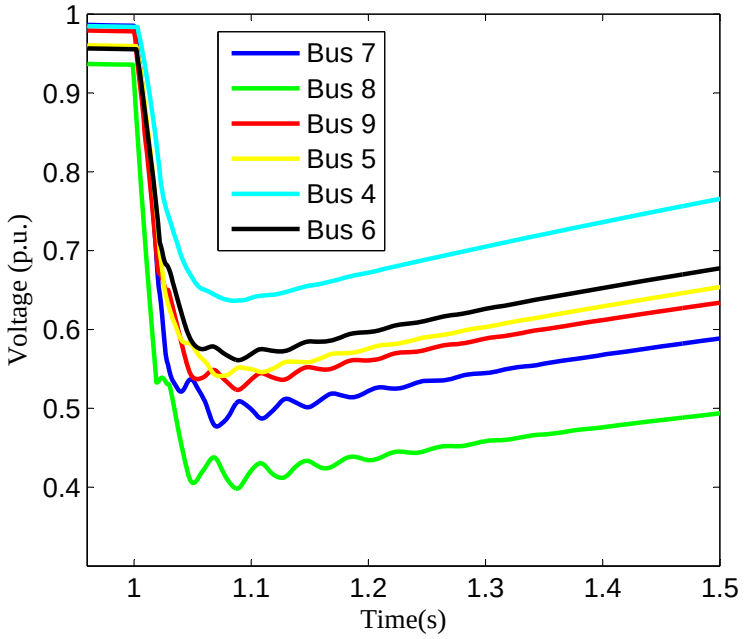

FIGURE 3.12: Magnitude of positive-sequence bus voltages.

bus 8. ϕ'_{1S}, ϕ_{1S} and ϕ_{1R} of line 7-8 along with their indices g'_{1S}, g_{1S} and g_{1R} are given in Figure 3.13(a) and (c) respectively. ϕ_{1S} and ϕ_{1R} of line 8-9 along with their indices g_{1S} and g_{1R} are given in Figure 3.13 (b) and (d) respectively. Neither of the two lines satisfy the conditions of FLI. So, this will be declared as non-fault event. This WABP algorithm performed accurately for load encroachment because during heavy loading

events, direction of current is not changed at both ends of the line like that of fault event.

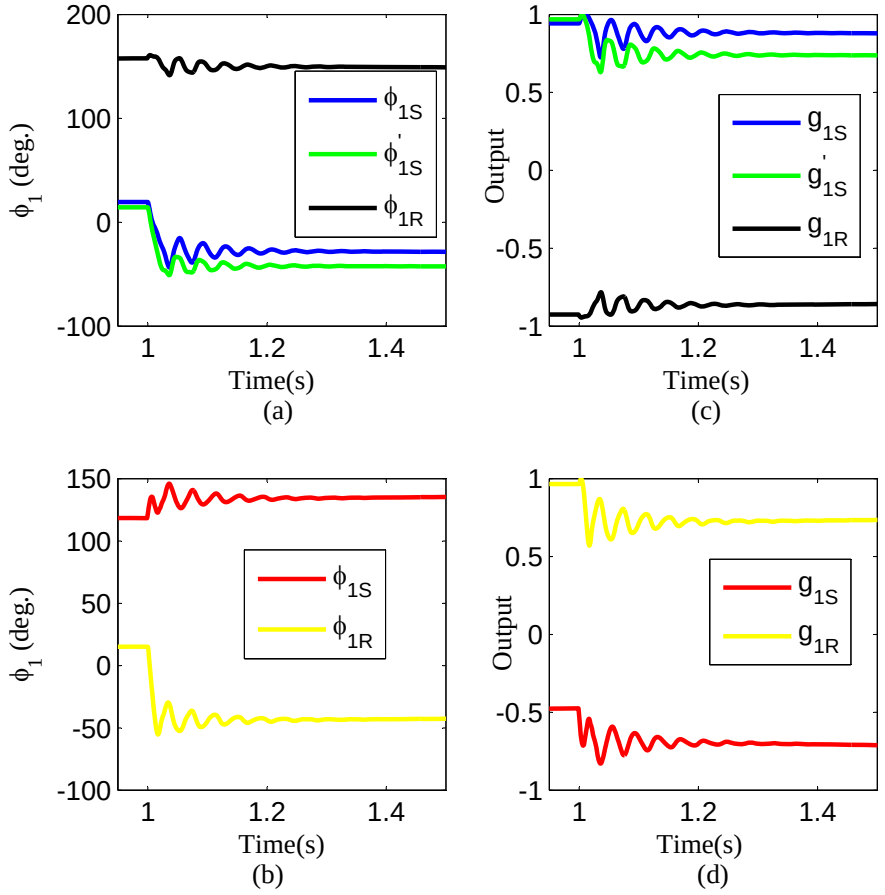

FIGURE 3.13: Performance during load encroachment. Angles at both ends of (a) Line 7-8 and (b) Line 8-9. Output indices of (c) Line 7-8 and (d) Line 8-9.

3.2.4 Performance during Power Swing

For creating power swing a three phase fault is simulated in line 7-5 at a distance of 200 km from bus 7 at 0.8 s and it is cleared by opening the contacts of line end breakers at 0.9 s. Power swing is introduced in the network due to removal of the line 7-5. During this event, positive-sequence impedance measured by relay at bus 7 enters the zone 3 operating region,so this would lead to false tripping of line 9-8. To check the performance of this method during power swing conditions, Figure 3.15 shows the plot of positive-sequence voltage magnitude. As bus 8 voltage has reduced below the threshold so it will trigger the FLI criteria for line 7-8 and 8-9. Plots corresponding to FLI are shown in Figure 3.16 and these lines do not satisfy the fault identification criteria and hence this condition will be declare as non-fault event.

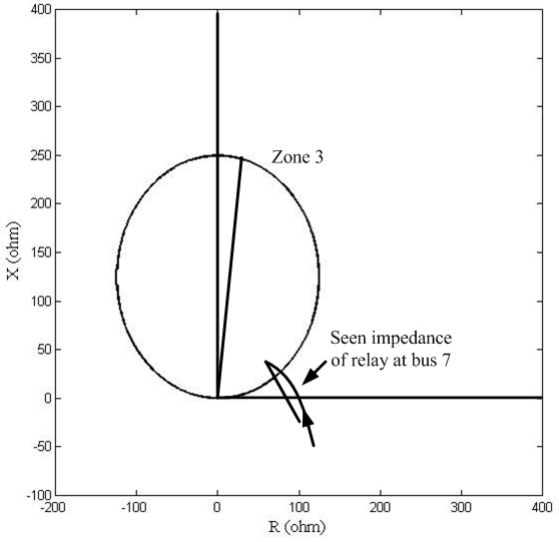

FIGURE 3.14: Trajectory of positive-sequence impedance measured by relay at bus-7 during power swing.

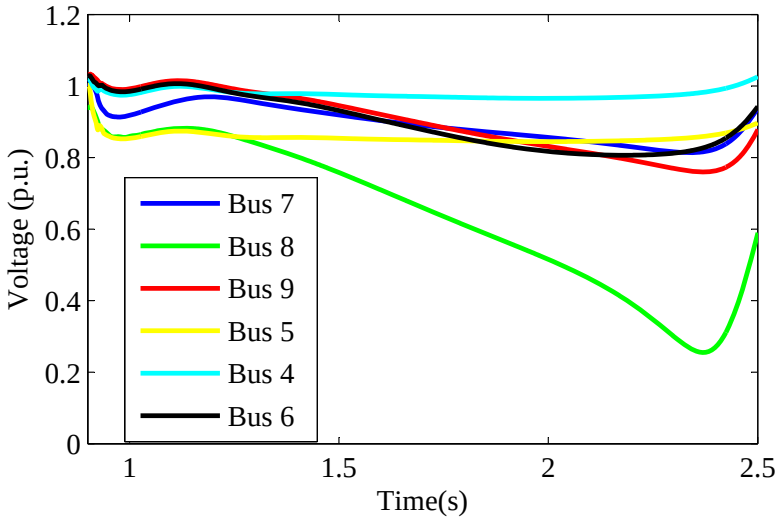

FIGURE 3.15: Magnitude of positive-sequence bus voltages.

3.2.5 Performance for Fault during Power Swing

A power swing is introduced in the system as described in previous section. To study the performance of this technique for faults during power swing, a line to ground is simulated in phase-A of line 7-8 at a distance of 100 km from bus 7 at 2.8 s. Figure shows the plot of negative-sequence voltage magnitude for unbalanced fault created in line 7-8. As bus 8 voltage has reached the threshold so it will trigger the FLI criteria for line 7-8 and 8-9. Plots corresponding to FLI are shown in figure and these lines do not satisfy the fault identification criteria and hence this condition will be declare as

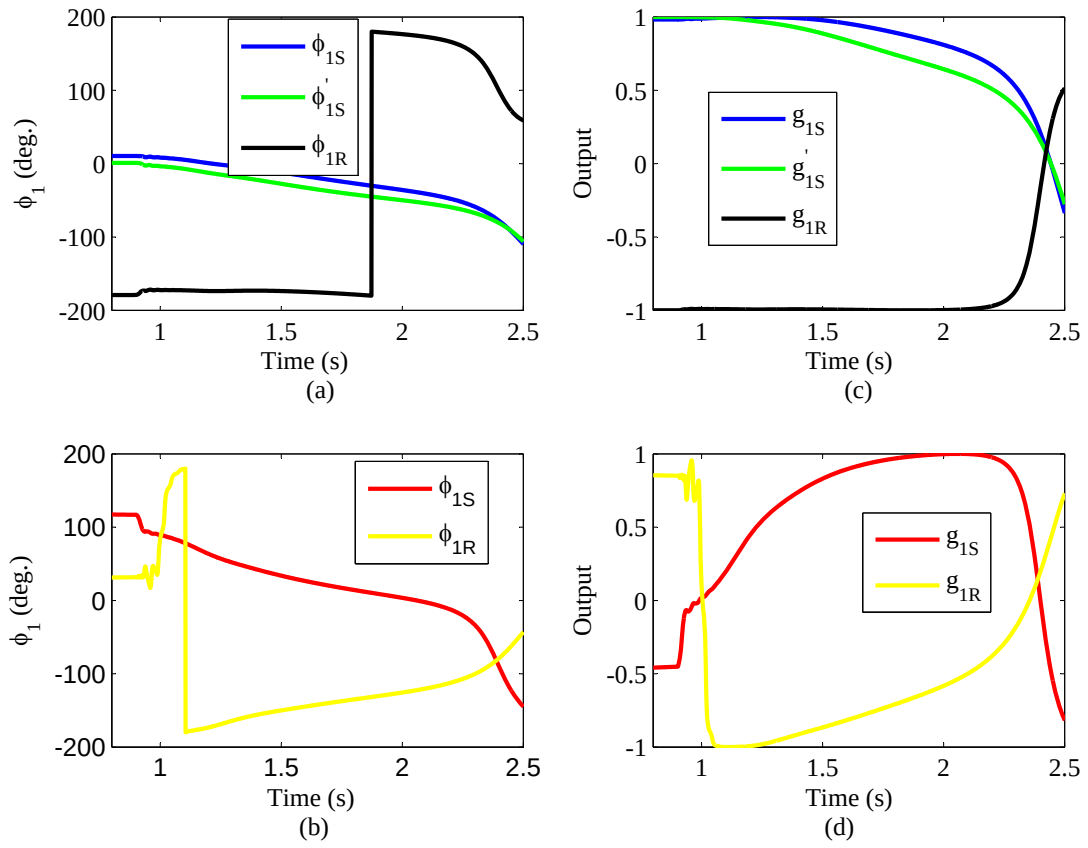

FIGURE 3.16: Performance during power swing. Angles at both ends of (a) Line 7-8 and (b) Line 8-9. Output indices of (c) Line 7-8 and (d) Line 8-9.

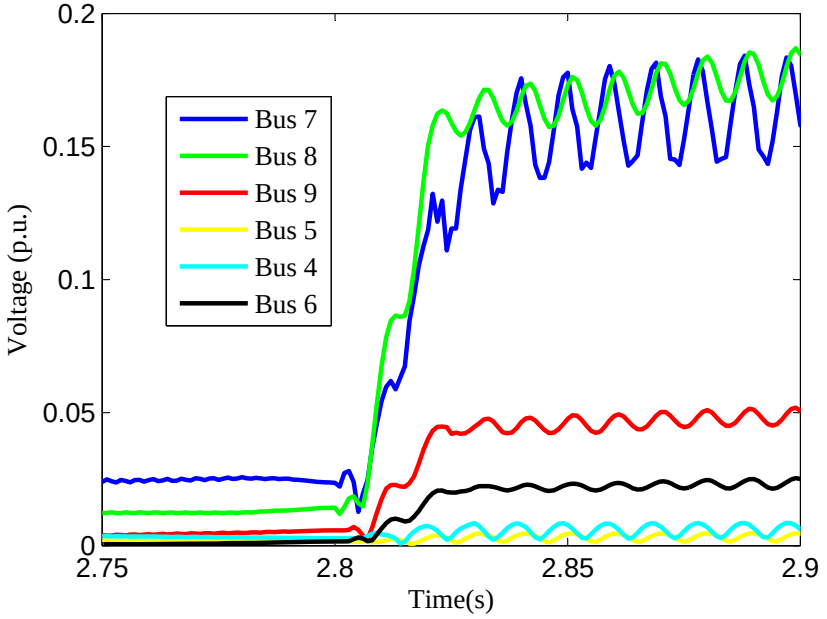

FIGURE 3.17: Magnitude of negative-sequence bus voltages.

non-fault event even though there is a fault in the system. So this technique finds it limitation for fault inception in the system during power swing condition.

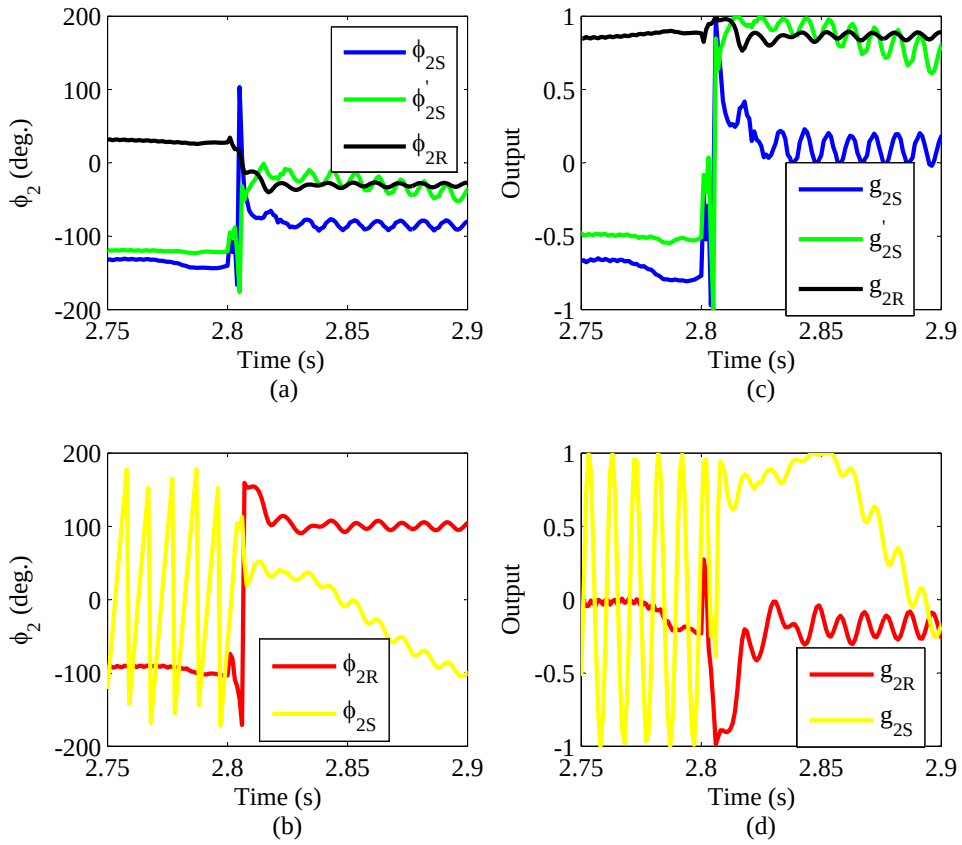

FIGURE 3.18: Performance for fault during power swing. Angles at both ends of (a) line 7-8 and (b) line 8-9. Output indices of (c) line 7-8 and (d) line 8-9.

Chapter 4

Fault Identification using WAMS during power swing

Under steady state operation of power system, load and generation balance each other. Sudden disturbances such as generator disconnection, transmission line switching and switching of large loads results in oscillating rotor angles of generators and causes power-flow swings. During power swing, large fluctuations occur in power between different regions of power network.

These oscillations may cause the distance relay to see an impedance which falls in its operating zone. This may cause mal-operation of the relay and will trip line during non-fault conditions. To ensure proper operation of distance relay, it is provided with power swing blocking (PSB) function [26]. However, relay is expected to detect the faults occurring during power swings. Different techniques have been proposed in literature for detecting faults during power swing condition. A technique using rate of change of resistance is given in [30], it distinguish between fault and power swing based on the fact that apparent resistance is varying during power swing and is constant during fault condition. A method based on magnitude of swing-center voltage is presented in [31]. A superimposed component of current based method is proposed in [32]. Performance of these algorithms has not been verified for power swing in transmission lines with series compensation. To minimize the impact of faults on power system operation, only effected section should be isolated. Conventional direction estimation techniques based on sequence components such as phase angle between positive-sequence component of

current and voltage, angle between positive sequence component of fault and pre fault current [33] cannot be used for fault direction estimation because of oscillation in voltage and current signals. These issues and drawback of existing technique gives a strong motivation to develop a new fault detection and faulted section identification during power swing condition using synchrophasor data for uncompensated and compensated transmission lines. Fault detection during power swing is a relatively slow process. Therefore, WAMS having dedicated communication network and PMUs with high reporting rates can be used for this application [34].

4.1 Fault Detection

Inception of fault during power swing is detected by using superimposed positive sequence power. The superimposed positive sequence power ($\Delta\vec{P}_1$) is calculated using superimposed voltage ($\Delta\vec{V}_1$) and current ($\Delta\vec{I}_1$) as expressed by (4.1)

$$|\Delta\vec{P}_1| = |\Delta\vec{V}_1 \times \Delta\vec{I}_1| \tag{4.1}$$

where, $\Delta\vec{V}_1 = \vec{V}_{1f} - \vec{V}_{1pre}$ and $\Delta\vec{I}_1 = \vec{I}_{1f} - \vec{I}_{1pre}$, $\vec{V}_{1f}$ and $\vec{I}_{1f}$ are positive-sequence component of fault voltage and current respectively. $\vec{V}_{1pre}$ and $\vec{I}_{1pre}$ are positive-sequence component of pre-fault voltage and current respectively. A positive value of $|\Delta\vec{P}_1|$ is the indication of fault detection. Hence, fault detection rule is specified as

$$|\Delta\vec{P}_1| > 0 \tag{4.2}$$

4.2 Faulted Section Estimation

For fault direction estimation, different algorithms are used for balanced and unbalanced faults. For balanced faults, angle between superimposed positive-sequence voltage and current is used. Phase angle ϕ_1 is defined in (4.3).

$$\phi_1 = \angle\Delta\vec{V}_1 - \angle\Delta\vec{I}_1 \tag{4.3}$$

where, superimposed positive sequence current is calculated as $\Delta\vec{I}_1 = \vec{I}_{1f} - \vec{I}_{1pre}$ and superimposed positive sequence voltage is calculated as $\Delta\vec{V}_1 = \vec{V}_{1f} - \vec{V}_{1pre}$, $\vec{V}_{1f}$ and $\vec{I}_{1f}$ are denoting positive sequence component of fault voltage and current, $\vec{V}_{1pre}$ and $\vec{I}_{1pre}$

are denoting positive sequence component of pre-fault voltage and current respectively. ϕ_1 is positive when fault is behind the relay location i.e. backward fault and it is negative when fault is ahead of the relay location i.e. forward fault [35]. This has been explained by drawing phasor diagram for forward and backward faults as shown in Figure 4.1.

For unbalanced faults angle between negative sequence superimposed voltage and

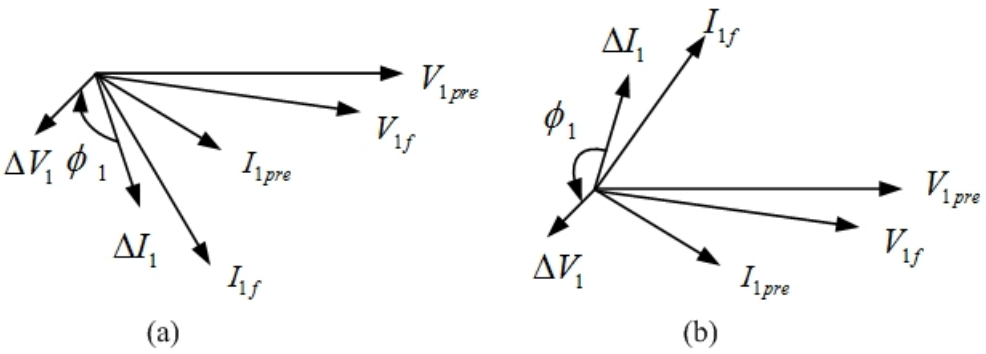

FIGURE 4.1: Phasor diagram of ϕ_1 (a)Forward fault (b) Backward fault.

current is used . Defining ϕ_2 as in (4.4)

$$\phi_2 = \angle\Delta\vec{V}_2 - \angle\Delta\vec{I}_2 \tag{4.4}$$

where, superimposed negative sequence voltage $\Delta\vec{V}_2 = \vec{V}_{2f} - \vec{V}_{2pre}$ and superimposed negative sequence current $\Delta\vec{I}_2 = \vec{I}_{2f} - \vec{I}_{2pre}$, $\vec{I}_{2f}$ and $\vec{V}_{2f}$ are denoting negative sequence component of fault current and voltage, $\vec{I}_{2pre}$ and $\vec{V}_{2pre}$ are denoting negative sequence component of pre-fault current and voltage respectively. ϕ_2 is positive for faults behind the relay location and negative for faults ahead of the relay location. Phasor diagram of ϕ_2 are shown in Figure 4.2.

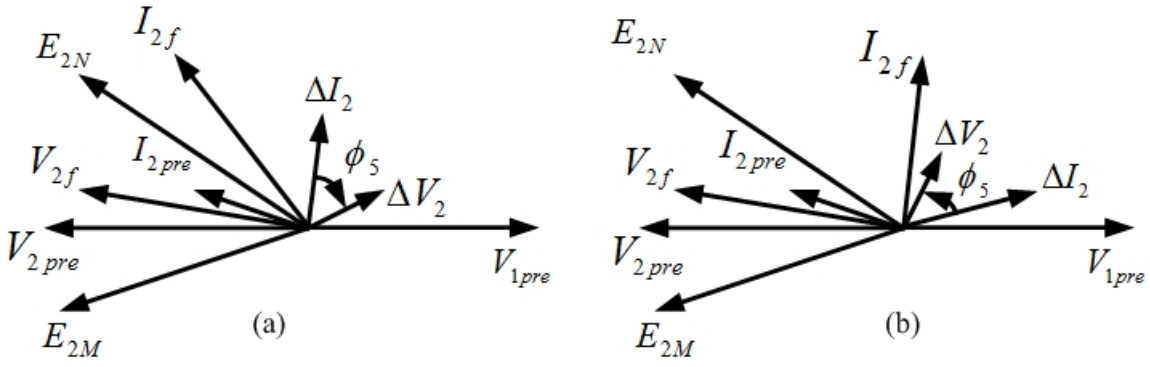

FIGURE 4.2: Phasor of ϕ_2 (a) Forward fault and (b) Backward fault.

When fault is identified in a system then fault direction estimation algorithm is activated. The buses in the system are arranged in decreasing order of their $|\Delta\vec{P}_1|$ value. All the lines connected to the bus with maximum value of $|\Delta\vec{P}_1|$ are checked for the fault based on the synchrophasor data received from the two ends of each line. It is assumed that relays at both terminals of the line are looking toward each other. So, the criteria for faulted line identification is that data from both ends of the line should indicate a forward fault. For non fault lines, data would indicate either one forward and one backward or both as backward fault. All the lines are scanned for this criteria till a faulted line is identified. So, the algorithm will declare a line as faulted line when

$$\begin{aligned} For\,Balanced\,Fault: &\quad \phi_{1S} < 0 \quad \cap \quad \phi_{1R} < 0 \\ For\,Unbalanced\,Fault: &\quad \phi_{2S} < 0 \quad \cap \quad \phi_{2R} < 0 \end{aligned} \tag{4.5}$$

where subscript S and R denotes sending and receiving end of the line respectively. To distinguish balanced and unbalanced faults magnitude of negative sequence current is used.

Performance of the proposed method is evaluated on a 400 kV 9 bus 3 machine modified WSCC-9 bus system. It is as shown in Figure 4.3. EMTDC/PSCAD has been used for simulating the 9 bus system. System data has been given in Appendix. Full cycle DFT has been used for estimating fundamental frequency sequence components. Phase-a is taken as the reference and sampling frequency of 1 kHz is used.

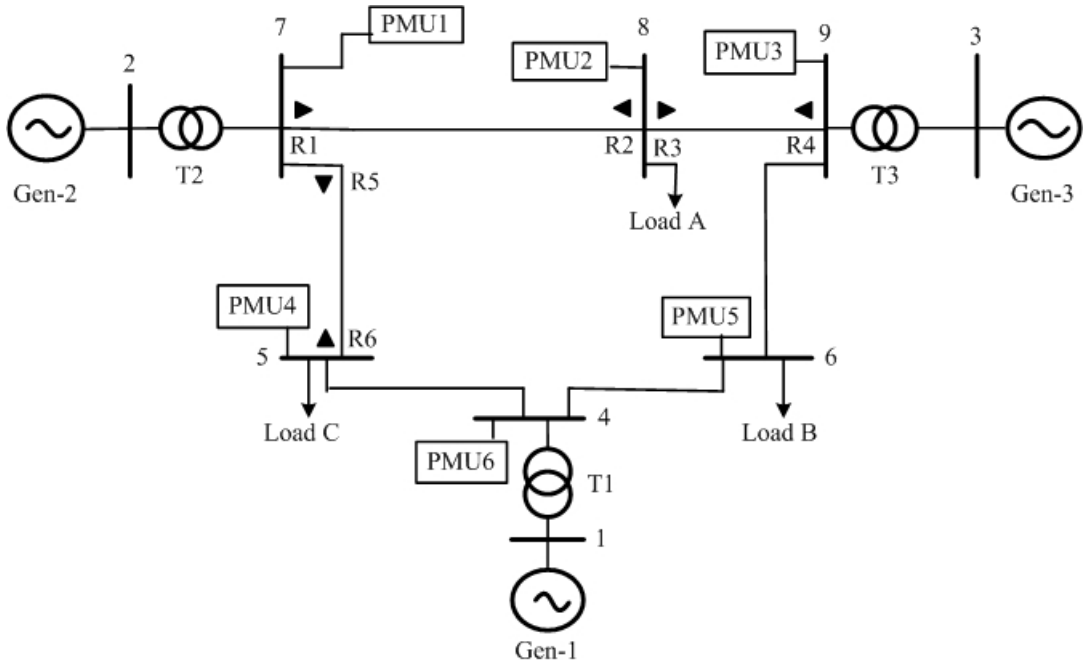

FIGURE 4.3: Modified WSCC 9 bus system single line diagram representation

4.3 Results

To evaluate the performance of proposed algorithm, results for different types of fault with and without series compensated are discussed. A three phase fault is simulated in line 5-7 at a distance of 200 km from bus 7 at 0.8 s and it is cleared at 0.9 s by opening the line breakers. Due to this, power swing is introduced in the system. Sampling frequency is 1 kHz. The CT ratio is taken as 500A/5A and PT ratio is taken as 400kV/110V. With power swing introduced in the system, performance of the proposed method is evaluated for different kinds of faults and conditions.

4.3.1 Results for Single Line to Ground Fault on Uncompensated Line

A phase-a to ground fault is created in line 7-8 of the system in Figure 4.3 at a distance of 160 km from bus 7 with fault resistance of 10 Ω at 2.5 s. Figure 4.4 shows plot of $|\Delta\vec{P}_1|$, positive values in the figure shows that inception of fault is identified. Value of $|\Delta\vec{P}_1|$ for different buses at 20 ms after the fault has occurred is summarized in Table 4.1 and corresponding to unbalanced fault on bus 7, values of ϕ_2 for line 7-8 and 7-5 is tabulated in Table 4.2.

TABLE 4.1: Value of $|\Delta\vec{P}_1|$ at different buses

	Bus 7	Bus 8	Bus 9	Bus 4	Bus 5	Bus 6
$\|\Delta\vec{P}_1\|$	14.1175	5.2088	1.5616	0.0163	0.1205	0.2191

TABLE 4.2: ϕ_2 for line 7-8 and 7-5

	R1	R2	R5	R6
ϕ_2	-84.0225	-41.3306	98.5144	-102.3332

As the value of $|\Delta\vec{P}_1|$ is maximum for bus 7, line 7-8 and 7-5 would be first checked for the fault. Figure 4.5 shows the plot of ϕ_2 at the ends of these two line and as ϕ_2 is negative at both ends of the line 7-8, so it is the faulted line.

4.3.2 Results for Double Line Fault on Uncompensated Line

A phase-b to phase-c fault is created in line 7-8 of the system at a distance of 280 km from bus 7 with fault resistance of 300 Ω at 2.5 s. Positive values of $|\Delta\vec{P}_1|$ in the Figure 4.6 shows that inception of fault is identified.

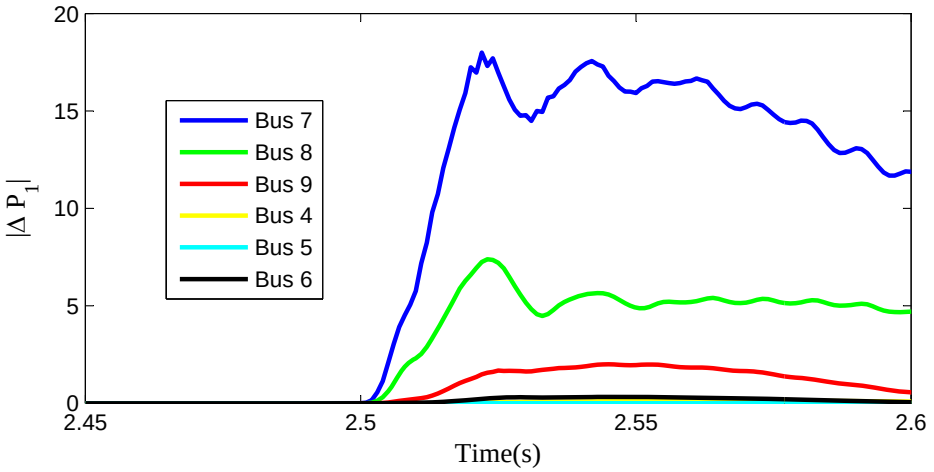

FIGURE 4.4: Variation of $|\Delta\vec{P}_1|$ at different buses for a L-g fault

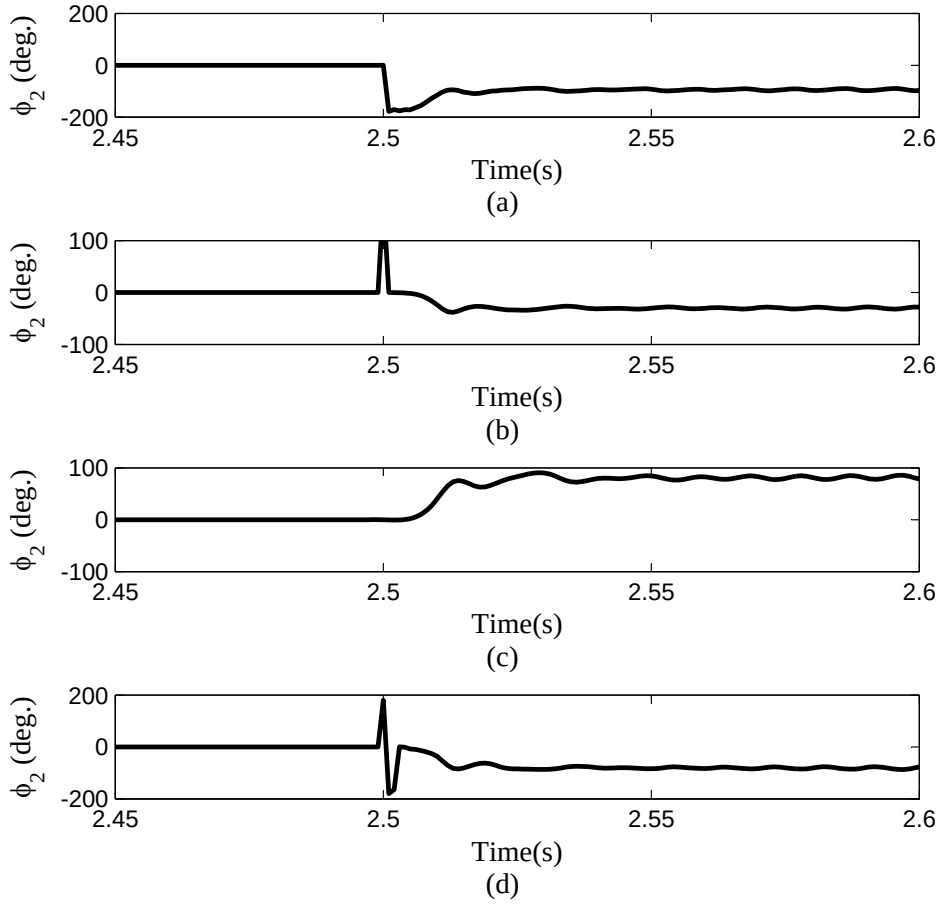

FIGURE 4.5: Variation of ϕ_2 for line 7-8: (a) R1 (b) R2 and line 7-5: (c) R5 (d) R6

Corresponding to maximum value of $|\Delta P_1|$ for bus 8, line 8-7 and 8-9 would be checked for unbalanced fault condition. Figure 4.7 shows the plot of ϕ_2 at the ends of these two line and based on faulted section identification criteria for ϕ_2,line 7-8 is declared as

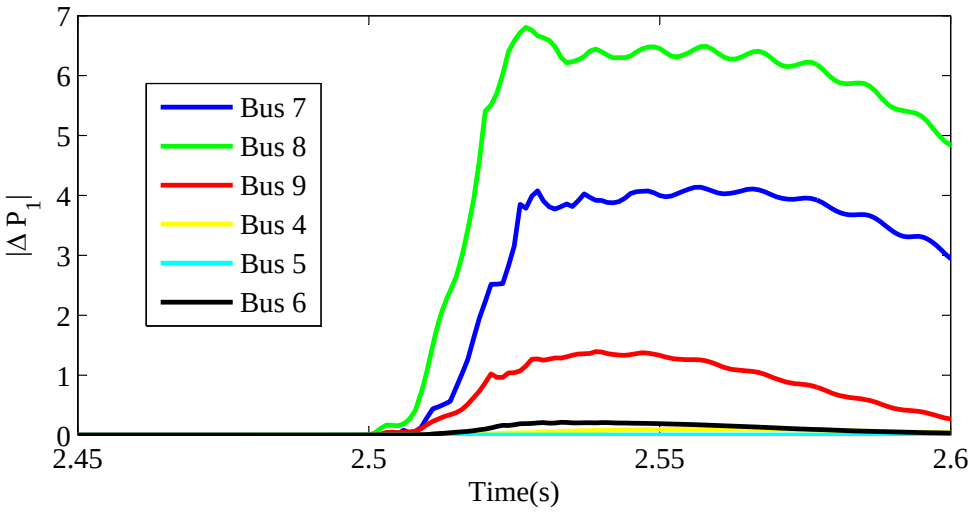

FIGURE 4.6: Variation of $|\Delta\vec{P}_1|$ at different buses for a L-L fault

faulted line.

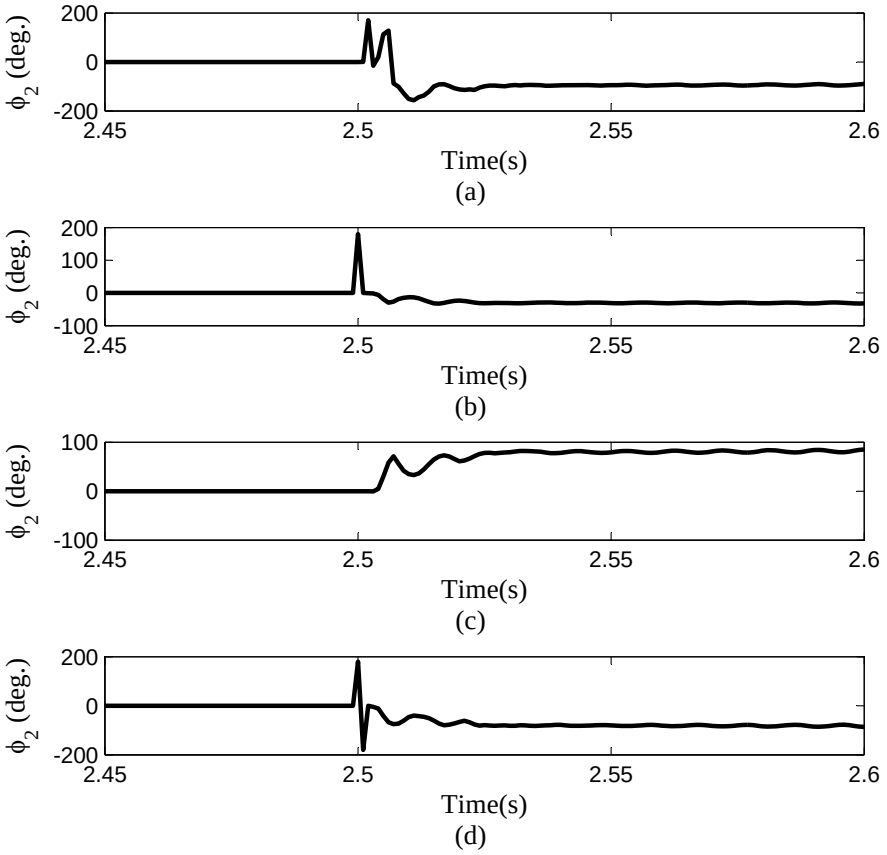

FIGURE 4.7: Variation of ϕ_2 for line 7-8: (a) R1 (b) R2 and line 8-9: (c) R3 (d) R4

4.3.3 Results for Three Phase Fault on Uncompensated Line

A three phase fault is created in line 7-8 at a distance of 200 km from bus 7 with fault resistance of 100 Ω at 2.5 s. Occurrence of fault in the system is clearly indicated by positive value of $|\Delta\vec{P}_1|$ in the Figure 4.8. Value of $|\Delta\vec{P}_1|$ for different buses at 20 ms after the fault has occurred is summarized in Table 4.3 and corresponding to balanced fault on bus 7, values of ϕ_1 for line 7-8 and 7-5 is tabulated in Table 4.4.

TABLE 4.3: Value of $|\Delta\vec{P}_1|$ at different buses

	Bus 7	Bus 8	Bus 9	Bus 4	Bus 5	Bus 6
$\|\Delta\vec{P}_2\|$	75.4833	40.7657	3.3072	0.0099	0.0247	0.0574

TABLE 4.4: ϕ_1 for line 7-8 and 7-5

	R1	R2	R5	R6
ϕ_1	-93.8883	-27.0994	63.2099	-67.1558

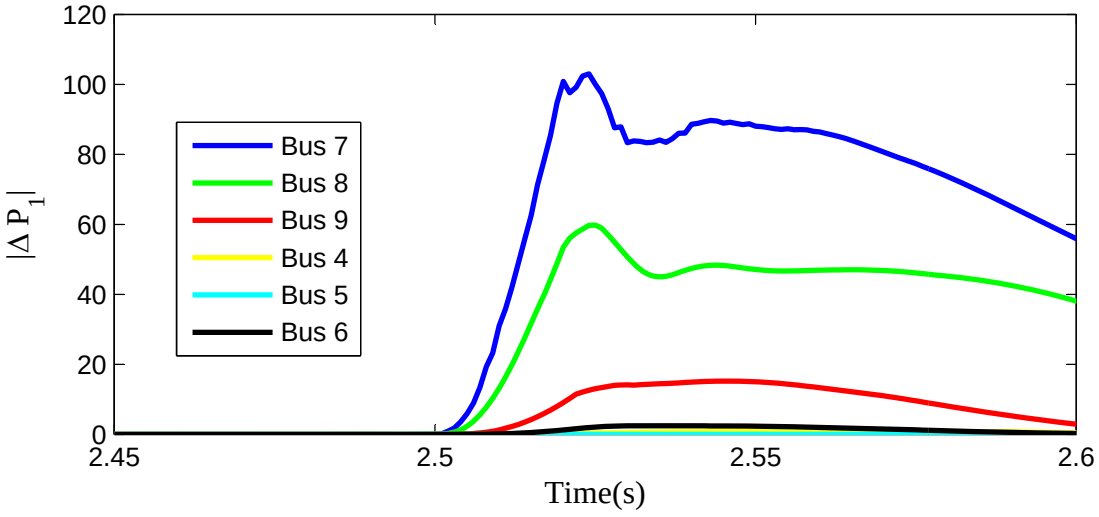

FIGURE 4.8: Variation of $|\Delta\vec{P}_1|$ at different buses for a three phase fault

As bus 7 has maximum value of $|\Delta\vec{P}_1|$, line 8-7 and 5-7 would be checked for fault condition. Figure shows the plot of ϕ_1 at the ends of these two line and based on fault criteria for ϕ_1,line 7-8 is declared as faulted line as shown in Figure 4.9.

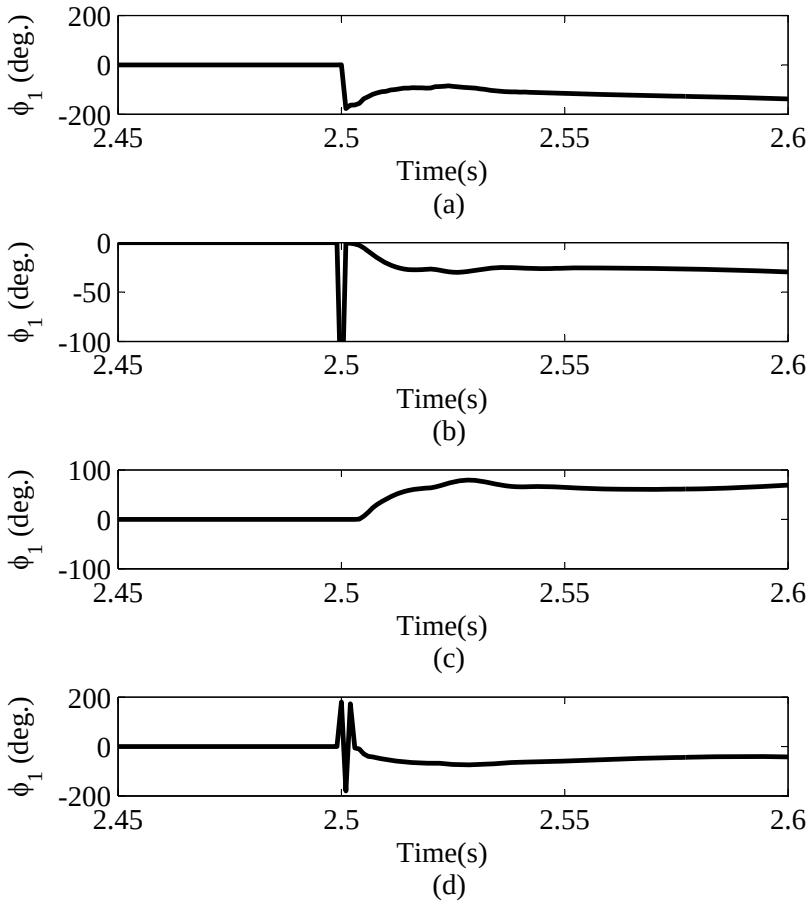

FIGURE 4.9: Variation of ϕ_1 for line 7-8: (a) R1 (b) R2 and line 7-5: (c) R5 (d) R6

4.3.4 Results for Single Line to Ground Fault on Series Compensated Line

Line 7-8 of Figure 4.1 is provided with 70% fixed series compensation and a phase-a to ground fault is created in it at a distance of 250 km from bus 7 with fault resistance of 50 Ω at 2.5 s. Figure 4.10 shows plot of $|\Delta\vec{P}_1|$, positive values in the figure shows that occurrence of fault is identified.

As the value of $|\Delta\vec{P}_1|$ is maximum for bus 7, line 7-8 and 7-5 would be first checked for the unbalanced fault. Figure 4.11 shows the plot of ϕ_2 at the ends of these two line and as ϕ_2 is negative at both ends of the line 7-8, so it is the faulted line.

4.3.5 Results for Double Line Fault on Series Compensated Line

A phase-b to phase-c fault is created in line 7-8 of the system at a distance of 160 km from bus 7 with fault resistance of 1 Ω at 2.5 s. Positive values of $|\Delta\vec{P}_1|$ in the Figure

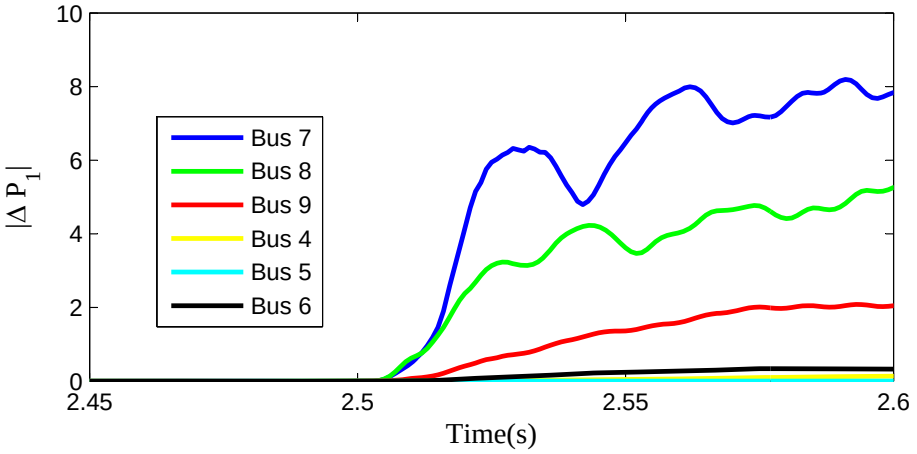

FIGURE 4.10: Variation of $|\Delta\vec{P}_1|$ at different buses for a L-g fault in series compensated line

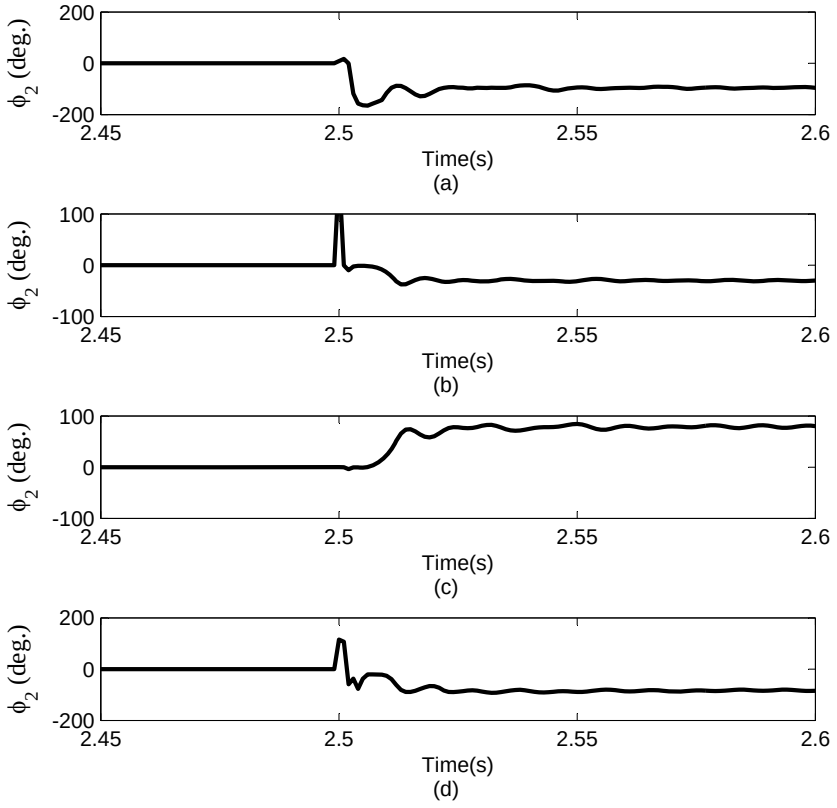

FIGURE 4.11: Variation of ϕ_2 for line 7-8: (a) R1 (b) R2 and line 7-5: (c) R5 (d) R6

4.12 shows that occurrence of fault is identified.

Corresponding to maximum value of $|\Delta\vec{P}_1|$ for bus 8, line 8-7 and 8-9 would be checked for unbalanced fault condition. Figure 4.13 shows the plot of ϕ_2 at the ends of these two line and based on fault criteria for ϕ_2, line 7-8 is declared as faulted line.

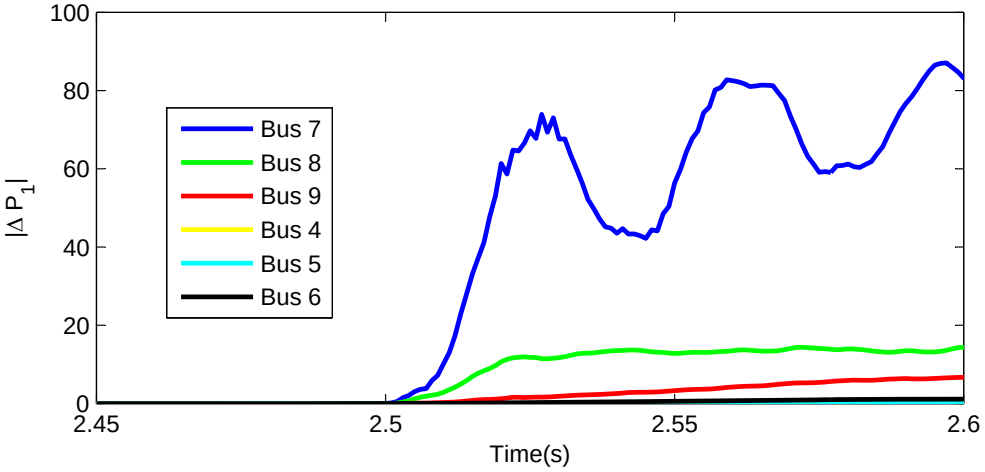

FIGURE 4.12: Variation of $|\Delta\vec{P_1}|$ at different buses for a L-L fault in series compensated line

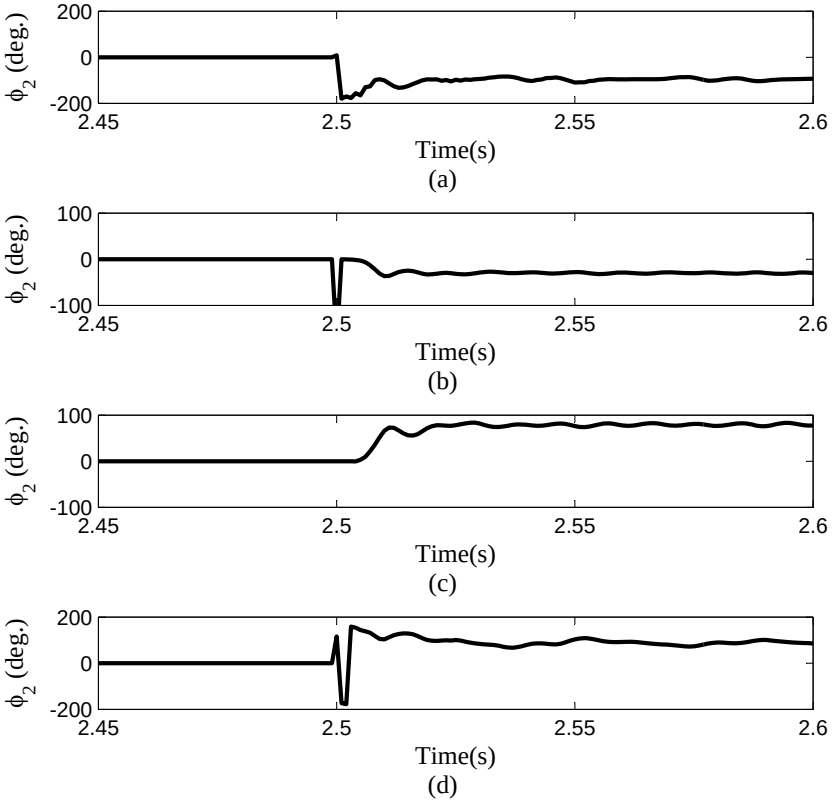

FIGURE 4.13: Variation of ϕ_2 for line 7-8: (a) R1 (b) R2 and line 7-5: (c) R5 (d) R6

4.3.6 Results for Three Phase Fault on Series Compensated Line

A three phase fault is created in line 7-8 at a distance of 20 km from bus 7 with fault resistance of 0.01 Ω at 2.5 s. Occurrence of fault in the system is clearly indicated by positive value of $|\Delta\vec{P_1}|$ in the Figure 4.14. As bus 7 has maximum value of $|\Delta\vec{P_1}|$, line

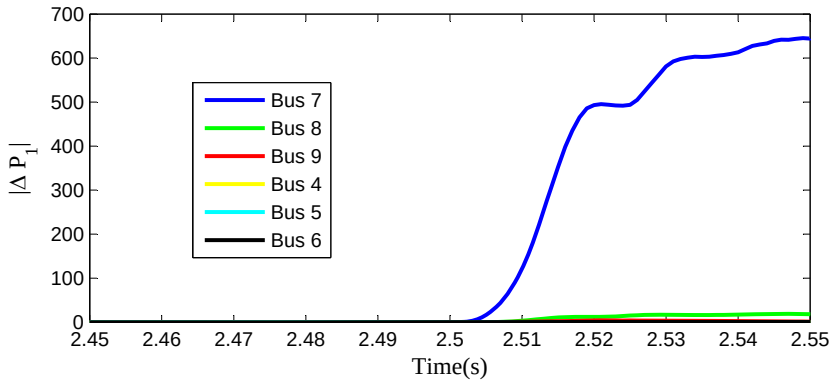

FIGURE 4.14: Variation of $|\Delta\vec{P}_1|$ at different buses for a three phase fault in series compensated line

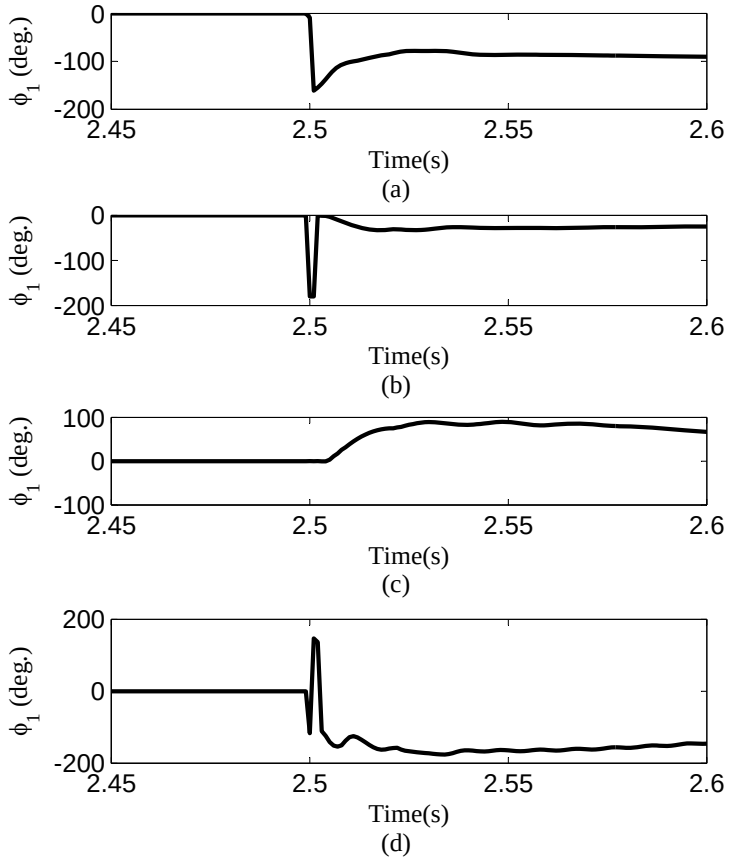

FIGURE 4.15: Variation of ϕ_1 for line 7-8: (a) R1 (b) R2 and line 7-5: (c) R5 (d) R6

8-7 and 7-5 would be checked for balanced fault condition. Figure shows the plot of ϕ_1 at the ends of these two line and based on fault criteria for ϕ_1, line 7-8 is declared as faulted line as shown in Figure 4.15.

Chapter 5

Fuzzy Integrated Protection Scheme

5.1 Feature Selection

Protection scheme studied in Chapter 3 is very complex for implementation in real time as different criteria has been used for different fault condition. Therefore in this chapter, a new protection scheme has been presented. Based on the study, different features are selected for developing an integrated data technique based on fuzzy logic. Behavior of each feature has been explained by drawing phasors for relay at bus L in the three bus system shown in Figure 5.1. For the relay under study, fault in line-2 is called forward fault and fault in line-1 is called backward fault. Each selected feature has some limiting conditions during which it fails to give correct decision. However, by integrating these features suitably, superior decision making model can be designed. A deterministic algorithm can not be used for integrating these features as these features have different variations for different conditions. Therefor, a fuzzy logic based integrating approach has been proposed.

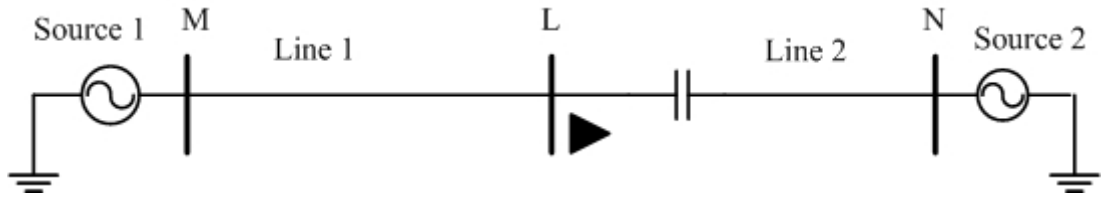

FIGURE 5.1: Power system network

5.1.1 Feature-1 (f1): Phase angle between positive-sequence component of fault current and fault voltage

The first feature is based on angle between positive sequence fault current and fault voltage. Defining $\phi_1 = \angle\vec{I}_{1f}$ - $\angle\vec{V}_{1f}$ where, $\vec{I}_{1f}$ is denoting positive sequence component of fault current and $\vec{V}_{1f}$ is denoting positive sequence component of fault voltage. For uncompensated line, this feature is positive for faults behind the relay location and negative for faults ahead of the relay location. Phasor diagram for ϕ_1 variation for backward fault is given in Figure 5.2(a) and Phasor corresponding to forward fault with voltage inversion is shown in Figure 5.2(b). Due to inversion, relay will see a fault current which is leading the fault voltage and it gives an illusion of a backward fault even though it is forward fault. Thus feature ϕ_1 has limitation during current/voltage inversion.

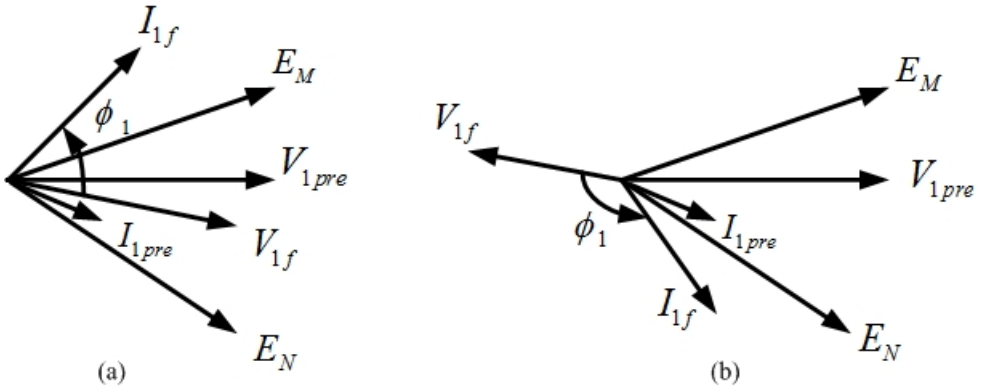

FIGURE 5.2: Phasor of ϕ_1 (a) Backward fault and (b) Forward fault with voltage inversion.

5.1.2 Feature-2 (f2): Phase angle between positive sequence component of fault current and prefault current

The second feature is based on angle between positive sequence fault current and prefault current. Defining $\phi_2 = \angle\vec{I}_{1f}$ - $\angle\vec{I}_{1pre}$ where, $\vec{I}_{1f}$ is denoting positive sequence

component of fault current and $\vec{I}_{1pre}$ is denoting positive sequence component of pre-fault current. For uncompensated line, this feature is positive for faults behind the relay location and negative for faults ahead of the relay location. Phasor diagram for ϕ_2 variation for backward fault is shown in Figure 5.3(a) and Phasor corresponding to forward fault with current inversion is given in Figure 5.3(b). Due to inversion, relay will see a fault current which is leading the pre-fault current same as that of backward fault. So this feature will give wrong decision. Thus feature ϕ_2 is not effected by voltage inversion but is effected during current inversion.

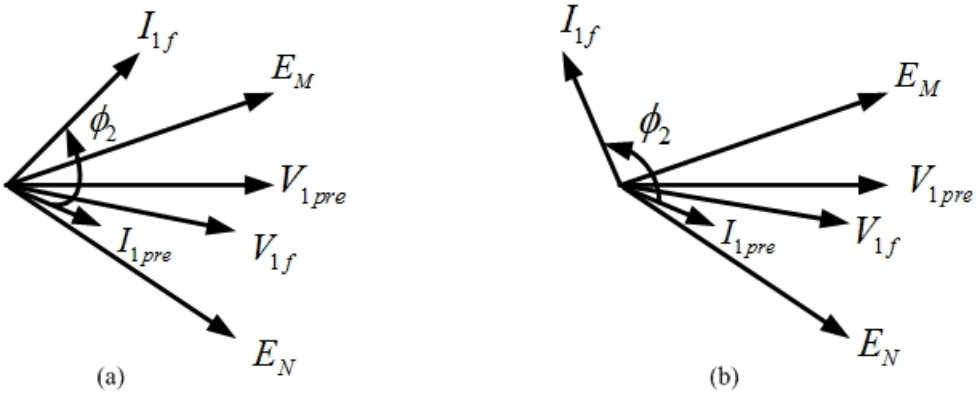

FIGURE 5.3: Phasor of ϕ_2 (a) Backward fault and (b) Forward fault with current inversion.

5.1.3 Feature-3 (f3): Phase angle between positive sequence superimposed voltage and current

The third feature uses the angle between positive sequence superimposed voltage and current. Defining $\phi_3 = \angle\Delta\vec{V}_1$ - $\angle\Delta\vec{I}_1$ where, superimposed positive sequence current is calculated as $\Delta\vec{I}_1 = \vec{I}_{1f} - \vec{I}_{1pre}$ and superimposed positive sequence voltage is calculated as $\Delta\vec{V}_1 = \vec{V}_{1f} - \vec{V}_{1pre}$, $\vec{V}_{1f}$ and $\vec{I}_{1f}$ are denoting positive sequence component of fault voltage and current, $\vec{V}_{1pre}$ and $\vec{I}_{1pre}$ are denoting positive sequence component of pre-fault voltage and current respectively. For uncompensated line, this feature is positive for faults behind the relay location and negative for faults ahead of the relay location. Phasor diagram for ϕ_3 variation for backward fault is shown in Figure 5.4(a), $\Delta\vec{I}_1$ lags the $\Delta\vec{V}_1$. When there is change is system loading, Figure 5.4(b) shows that $\Delta\vec{I}_1$ leads $\Delta\vec{V}_1$. I'_{1pre} and I''_{1pre} are currents for old and new load conditions respectively. Thus it can be seen that relay will declare a load change condition as fault condition which is undesirable. This feature performs reliably for current and voltage inversion.

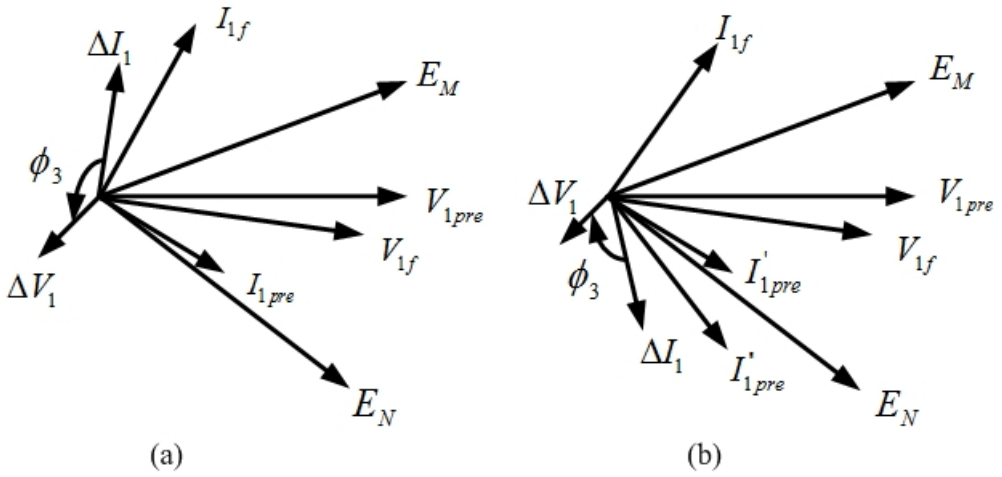

FIGURE 5.4: Phasor of ϕ_3 (a) Backward fault and (b) For change in load.

5.1.4 Feature-4 (f4): Phase angle between negative-sequence component of fault current and fault voltage

The forth feature is based on angle between negative sequence fault current and fault voltage. Defining $\phi_4 = \angle\vec{I}_{2f}$ - $\angle -\vec{V}_{2f}$ where,$\vec{I}_{2f}$ is denoting negative sequence component of fault current and $\vec{V}_{2f}$ is denoting negative sequence component of fault voltage. For uncompensated line, this feature is positive for faults behind the relay location and negative for faults ahead of the relay location. Phasor diagram for ϕ_4 variation for backward fault is shown in Figure 5.5(a). Phasor corresponding to forward fault with voltage inversion is given in Figure 5.5(b). Due to inversion, relay will see a fault current which is leading the fault voltage and it gives an illusion of a backward fault even though it is forward fault. Thus feature ϕ_4 is used because positive sequence based components find limitations during high resistance unbalanced faults, but it is valid only for unbalanced faults as presence of negative-sequence components during balanced conditions is negligible and it also has limitation during current/voltage inversion.

5.1.5 Feature-5 (f5): Phase angle between negative sequence superimposed voltage and current

The last feature uses the angle between negative sequence superimposed voltage and current. Defining $\phi_5 = \angle\Delta\vec{V}_2$ - $\angle\Delta\vec{I}_2$ where, superimposed negative sequence voltage $\Delta vecV_2 = \vec{V}_{2f} - \vec{V}_{2pre}$ and superimposed negative sequence current $\Delta\vec{I}_2 = \vec{I}_{2f} - \vec{I}_{2pre}$, $\vec{I}_{2f}$ and $\vec{V}_{1f}$ are denoting negative sequence component of fault current and voltage, $\vec{I}_{2pre}$ and $\vec{V}_{2pre}$ are denoting negative sequence component of pre-fault current and voltage

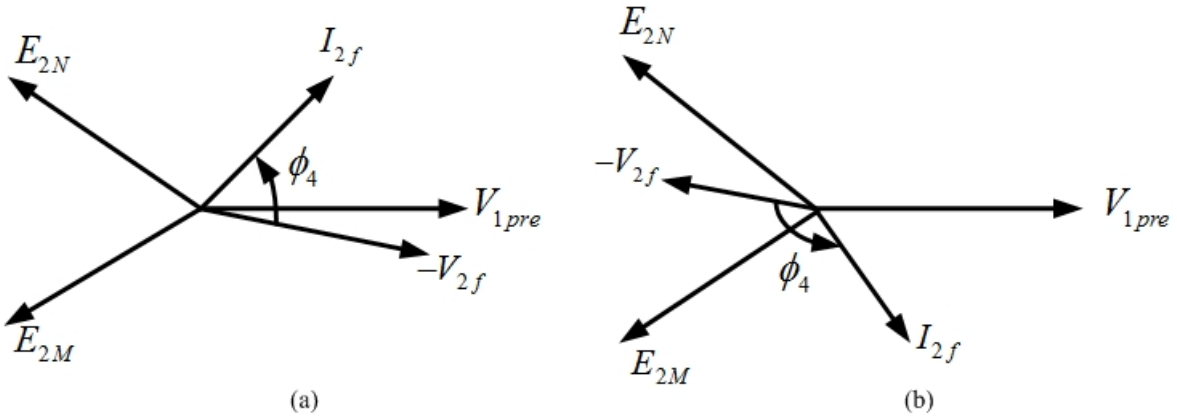

FIGURE 5.5: Phasor of ϕ_4 (a) backward fault and (b) forward fault with voltage inversion.

respectively. For uncompensated line, this feature is positive for faults behind the relay location and negative for faults ahead of the relay location. Phasor diagram for ϕ_5 are shown in Figure 5.6.

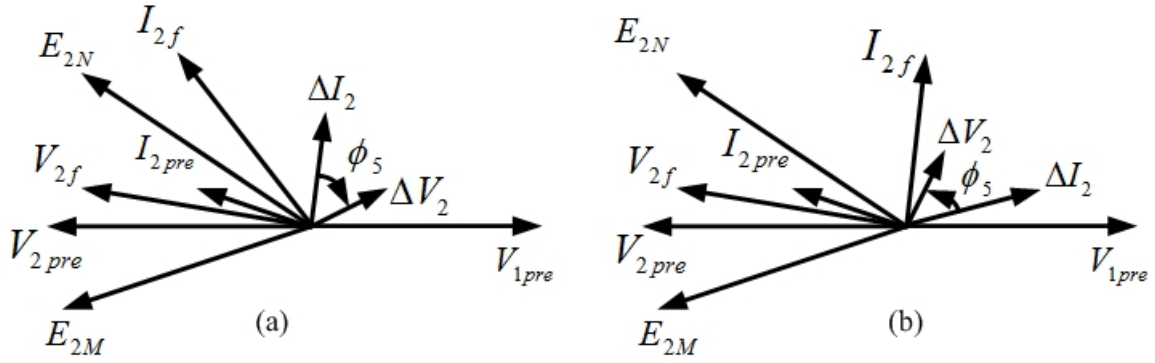

FIGURE 5.6: Phasor of ϕ_5 (a) Forward fault and (b) Backward fault.

5.2 Proposed Multicriteria Fuzzy Decision Technique using WAMS

Features discussed in the previous section are combined in fuzzy decision system to obtain more efficient and reliable faulted element identification technique. The variation of these features is studied for different conditions, types of faults and locations, this experience is then used for designing the fuzzy system.

Fuzzy IF-THEN rules for a classification problem with "k" attributes can be written as rule D_i: If a_1 is Y_{i1} and a_2 is Y_{i2} and..... a_k is Y_{ik} then the class is X_i, i = 1,2,3,4,.....,N

where A = (a_1, a_2, ..., a_k) is k-dimensional pattern vector. Y_{ij} is the antecedent linguistic value such as large positive/equal zero (j = 1, 2, ..., k), X_i is one of the consequent output class and number of fuzzy IF-THEN rules is represented by N. The compatibility grade $\mu_i(A)$ of the rule D_i is determined by using the minimum operation

$$\mu_i(A) = min\{\mu_{i1}(a_1), \mu_{i2}(a_2).....\mu_{ik}(a_k)\} \tag{5.1}$$

where $\mu_{ij}(a_j)$ is the membership function of the antecedent linguistic value Y_{ij}. An input vector is classified based on a single winner rule R_{i*} given by [36]

$$\mu_{i*}(A) = max\{\mu_i(A) : i = 1, 2, ...N\} \tag{5.2}$$

However, in a case more than one rules have same maximum value of compatibility grade for a particular input vector then each of the these selected rule votes for their output class and finally the class having the maximum votes is declared as the output and in case two output class have same votes then that input vector is discarded.
Based on the behavior of the features, membership function of the Fuzzy logic system (FLS) are finalized. Using the knowledge of the feature variation for different system conditions and different types of faults, range of membership functions are decided. Each feature is divided into five fuzzy set; "LN" represents large negative, "LP" represents large positive "SN" represents small negative, "SP" represents small positive and "EZ" represents equal zero. Fuzzy membership function for first feature(f1) is shown in Figure. In FLS, final output is decided by fuzzy IF-THEN rules which are frames based on feature variations for fault and normal conditions. For the designed FLS, fourteen rules have been framed. These rules are as follows:

1. IF f1 is EZ and f2 is EZ and f3 is SN and f4 is SN and f5 is SN THEN Output is 1.
2. IF f1 is EZ and f2 is SN and f3 is SN and f4 is SN and f5 is SN THEN Output is 1.
3. IF f1 is EZ and f2 is EZ and f3 is LN and f4 is SN and f5 is SN THEN Output is 1.
4. IF f2 is EZ and f3 is EZ and f5 EZ THEN Output is 0.
5. IF f1 is SN and f2 is SN and f3 is SN THEN Output is 1.

6. IF f1 is SP and f2 is EZ and f3 is SN THEN Output is 1.
7. IF f1 is EZ and f2 is SN and f3 is SN THEN Output is 1.
8. IF f1 is EZ and f2 is EZ and f3 is LN THEN Output is 0.
9. IF f3 is LN and f3(other end of line) is LN and f1 is EZ and f1(other end of line) is EZ then Output is 0.
10. IF f1 is SP and f2 is SP and f3 is EZ THEN Output is 1.
11. IF f1 is EZ and f2 is EZ and f3 is SP and f4 is SP and f5 is SP THEN Output is 1.
12. IF f1 is SP and f2 is EZ and f3 is EZ and f4 is SP and f5 is SP THEN Output is 0.
13. IF f1 is SP and f2 is EZ and f3 is SP and f4 is SP and f5 is SP THEN Output is 0.
14. IF f1 is EZ and f2 is SP and f3 is EZ and f4 is SP and f5 is SP THEN Output is 1.

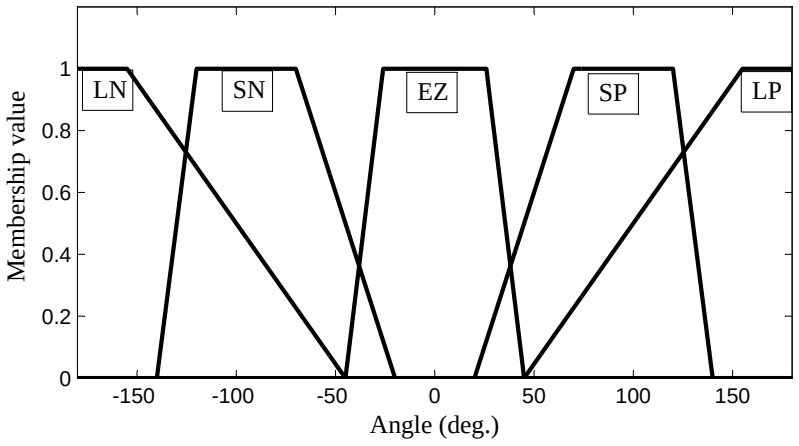

FIGURE 5.7: Fuzzy membership function of feature 1.

5.3 Results

Performance of the proposed technique is evaluated on a 400 kV 9 bus 3 machine modified WSCC-9 bus system. It is shown in Figure 3.1. EMTDC/PSCAD has been used for simulating the 9 bus system. System data has been given in Appendix. Availability of the PMUs at each bus of the system is assumed. Full cycle DFT has been used for estimating fundamental frequency sequence components. Phase-a is taken as the reference and sampling frequency of 1 kHz is used. The phasor information from each end of the lines is feed to FLS, and convention used is that the output of FLS should be

"1" if it predicts a fault condition and "0" if it predict a non fault condition. When FLS gives "1" as output for both ends of the line, then that line would be declared as the faulted line otherwise it is declared as non-fault. So faulted line declaration condition can be stated as

$$(Output_S = 1) \cap (Output_R = 1) \tag{5.3}$$

where, $Output_S$ is the predicted outputs for sending end and $Output_R$ is the predicted output for receiving end of the transmission line.

5.3.1 Results for Single Line to Ground Fault on Uncompensated Line

For evaluating the performance of proposed method for high resistance far end fault, a L-g fault is simulated in phase-a of line 7-8 at a distance of 200 km from bus 7 with fault resistance of 300 Ω at 1 s. Features discussed in previous section are given as input to the FLS for determining the faulted line. For relay close to bus 7 on line 7-8, first and second feature belongs to the set EZ, third, forth and fifth feature belongs to the set SN. For relay close to bus 8 on line 7-8, first and second feature belongs to the set EZ, third, forth and fifth feature belongs to the set SP. Variation of these features for both ends of line 7-8 is shown in Figure 5.8 and 5.9.

Output decision for line 7-8 and 8-7 are as shown in Figure 5.10. It shows that FLS

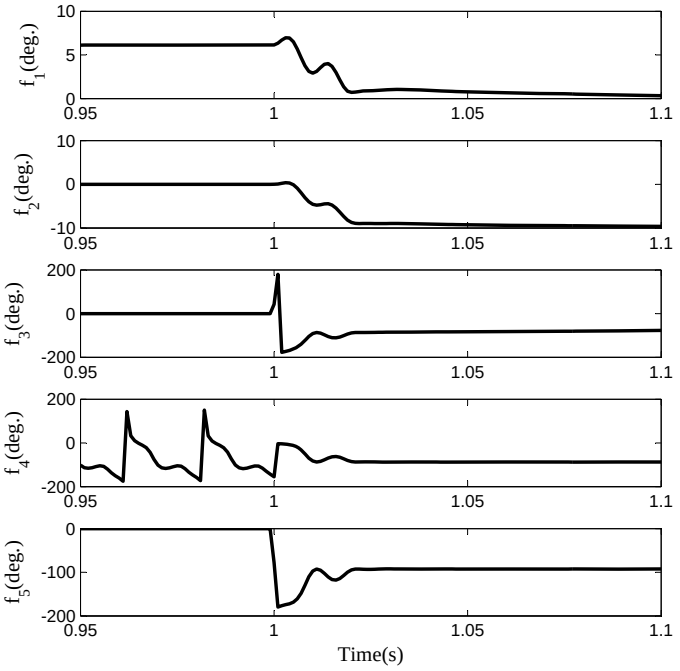

FIGURE 5.8: Variation of selected features at terminal of line 7-8 close to bus 7 for L-g fault

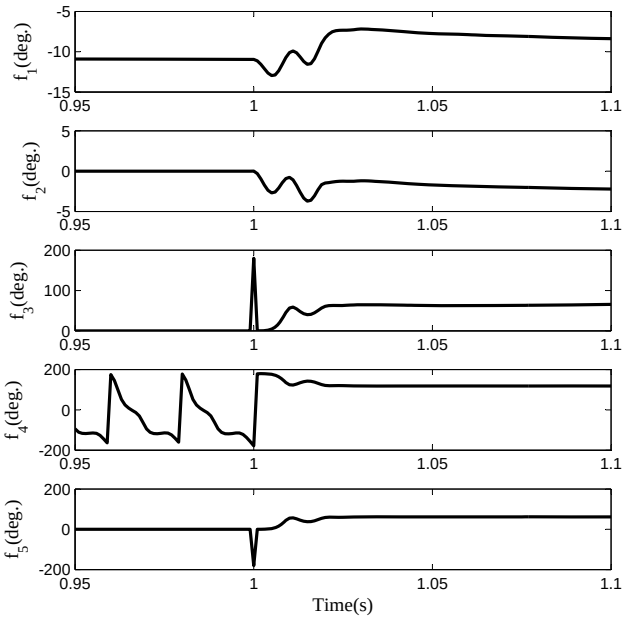

FIGURE 5.9: Variation of selected features at terminal of line 7-8 close to bus 8 for L-g fault

has given output as "1" for both ends of line 7-8 and output as "0" for both ends of line 8-9. So based on fault element identification criteria given in 5.3, line 7-8 is correctly declared as faulted line.

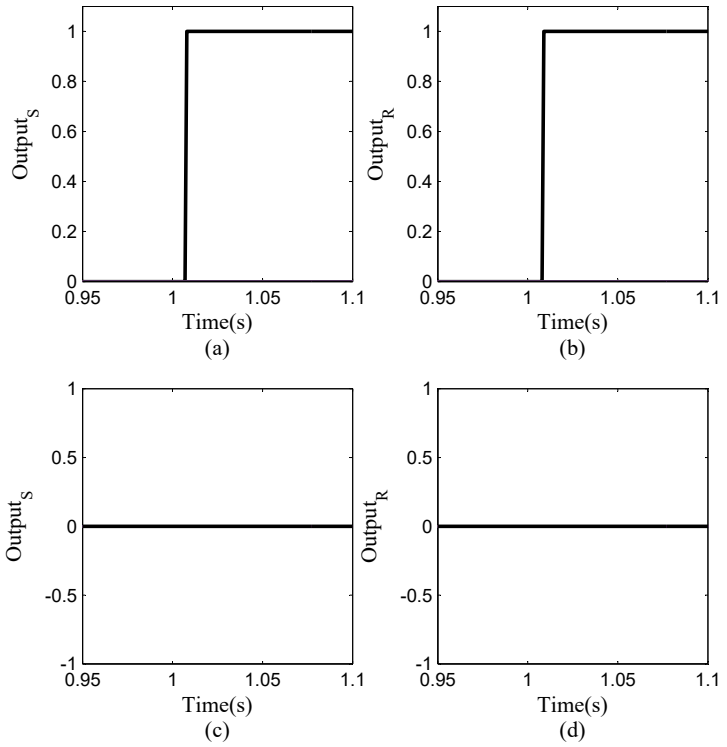

FIGURE 5.10: Performance for L-g fault on uncompensated line (a) and (b) Line 7-8, (c) and (d) Line 8-9.

5.3.2 Results for Double Line Fault on Uncompensated Line

A phase-b to phase-c fault is created in line 7-8 of the system at a distance of 100 km from bus 7 with fault resistance of 100 Ω at 1 s. Selected Features are given as input to the FLS. For relay close to bus 7 on line 7-8, first and second feature belongs to the set EZ, third, forth and fifth feature belongs to the set SN. For relay close to bus 8 on line 7-8, first feature belong to the set EZ and second feature belongs to the set SP, third feature belong to the set EZ, forth and fifth feature belongs to the set SP. Plots of these features for both ends of line 7-8 is shown in Figure 5.11 and 5.12.

Output decision for line 7-8 and 8-7 are as shown in Figure 5.13. It shows that FLS

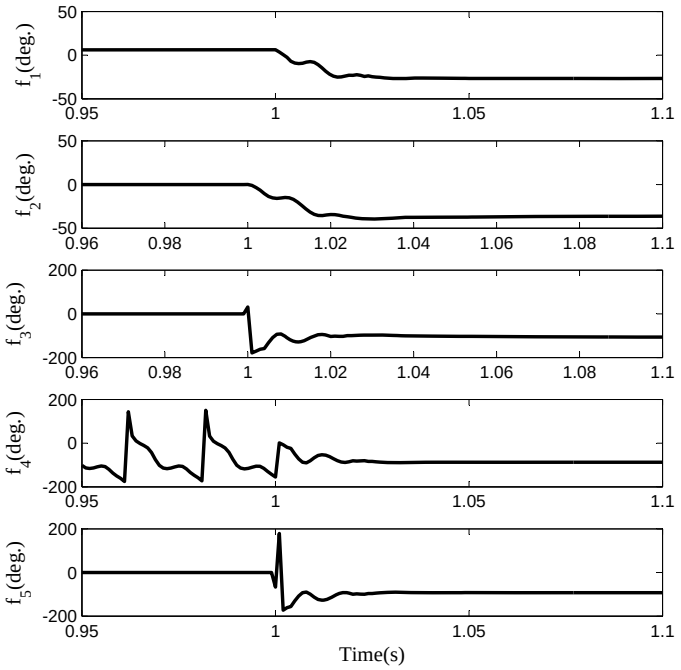

FIGURE 5.11: Variation of selected features at terminal of line 7-8 close to bus 7 for L-L fault

has given output as "1" for both ends of line 7-8 and output as "0" for both ends of line 8-9. So based on fault element identification criteria given in 5.3, line 7-8 is correctly declared as faulted line.

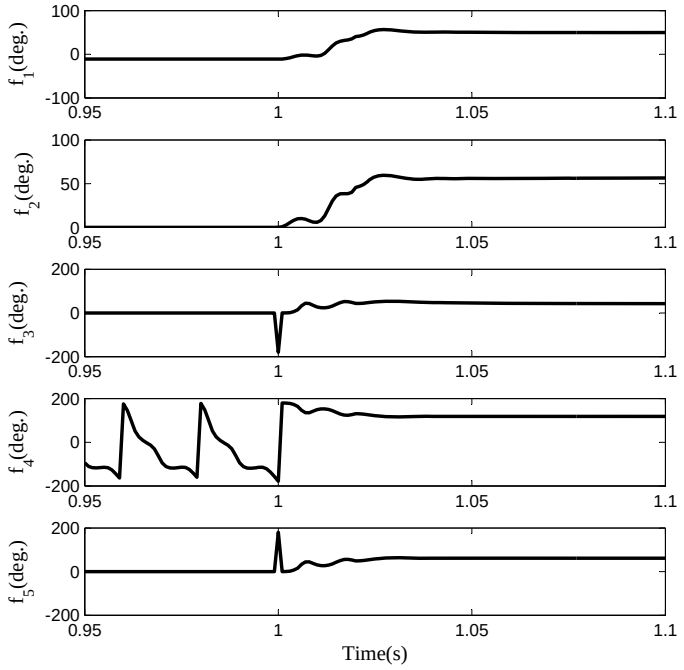

FIGURE 5.12: Variation of selected features at terminal of line 7-8 close to bus 8 for L-L fault

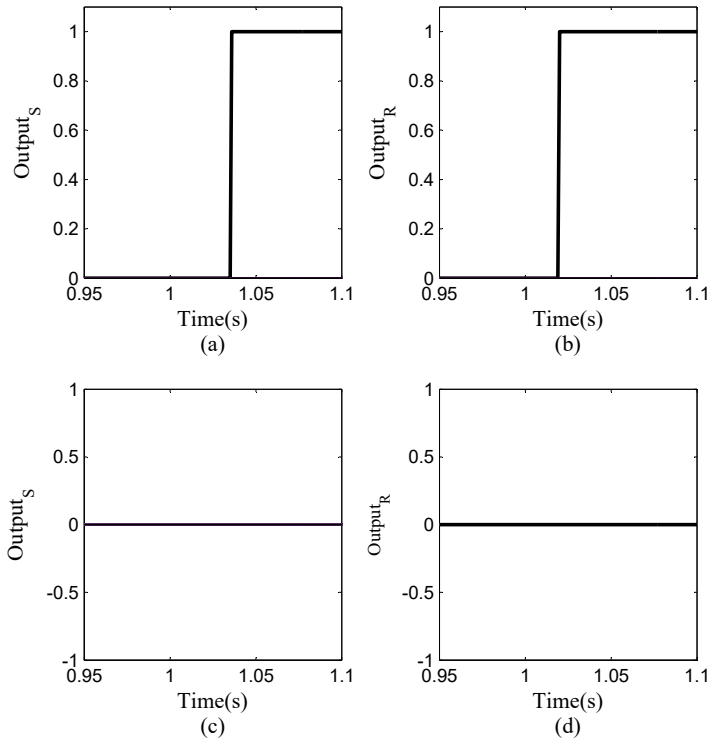

FIGURE 5.13: Performance for L-L fault on uncompensated line (a) and (b) Line 7-8, (c) and (d) Line 8-9.

5.3.3 Results for Three Phase Fault on Uncompensated Line

To analyze the performance of proposed technique for balance fault, a three phase fault is simulated on line 7-8 at a distance of 150 km from bus 7 with fault resistance of 0.1 Ω at 1 s. Selected Features are given as input to the FLS for determining the faulted line. For relay close to bus 7 on line 7-8, first, second and third feature belongs to the set SN. For relay close to bus 8 on line 7-8, first and second feature belongs to the set SP, third feature belongs to the set EZ. Variation of these features for both ends of line 7-8 is shown in Figure 5.14 and 5.15.

Output decision for line 7-8 and 8-7 are as shown in Figure 5.16. It shows that FLS

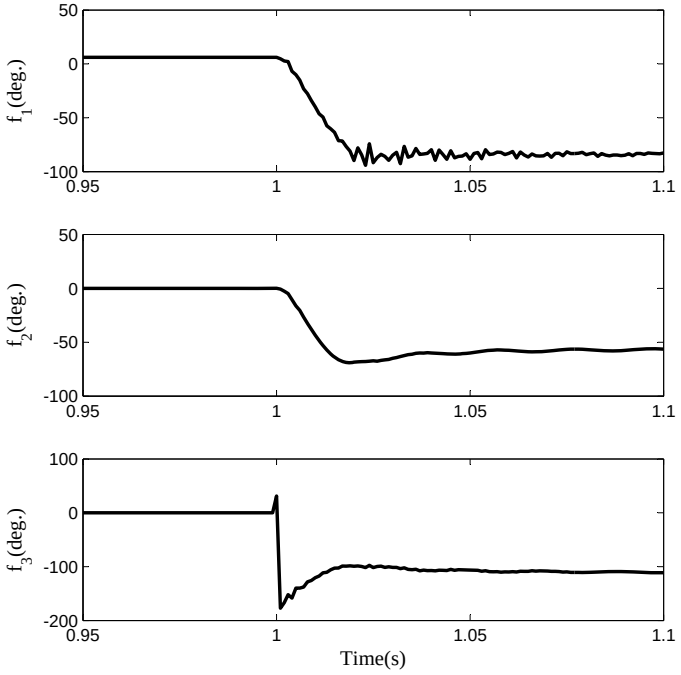

FIGURE 5.14: Variation of selected features at terminal of line 7-8 close to bus 7 for 3 ϕ fault

has given output as "1" for both ends of line 7-8 and output as "0" for both ends of line 8-9. So based on fault element identification criteria given in 5.3, line 7-8 is correctly declared as faulted line.

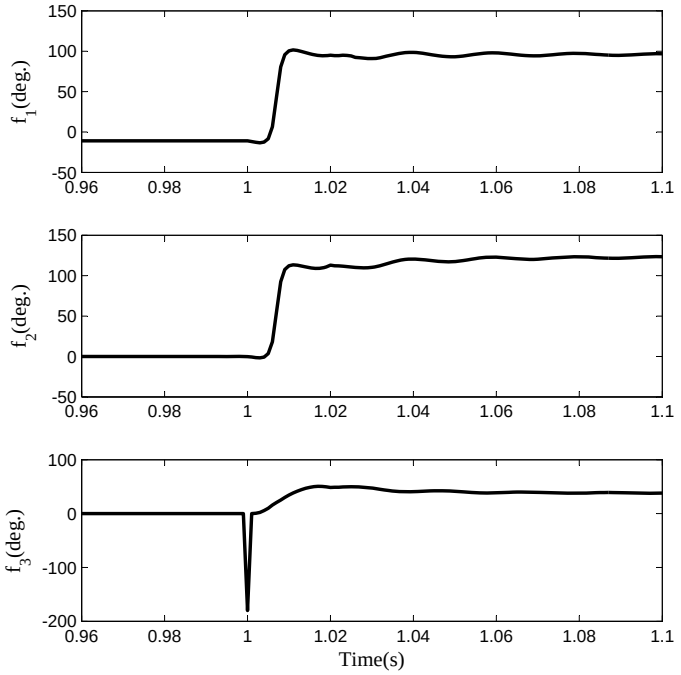

FIGURE 5.15: Variation of selected features at terminal of line 7-8 close to bus 8 for 3 ϕ fault

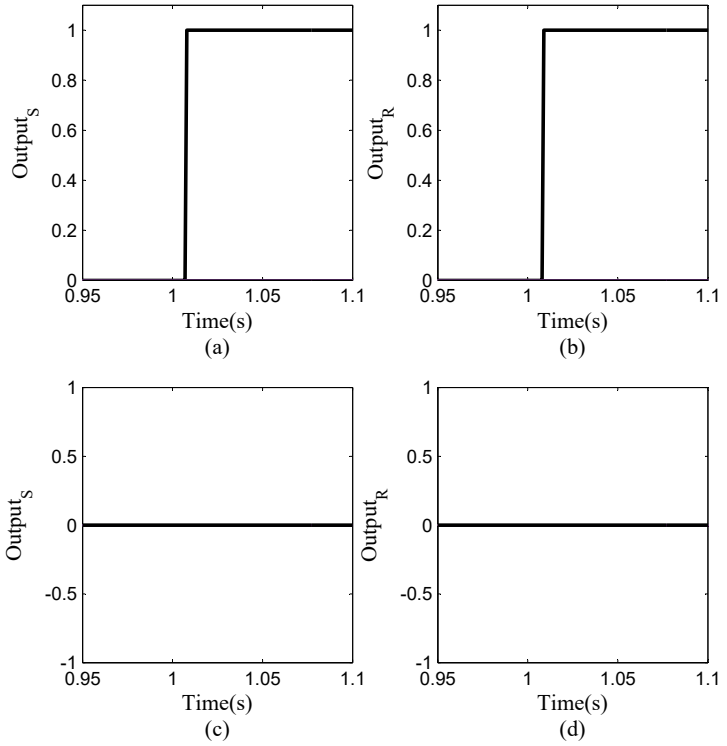

FIGURE 5.16: Performance for three phase fault on uncompensated line (a) and (b) Line 7-8, (c) and (d) Line 8-9.

5.3.4 Results for Single Line to Ground Fault on Series Compensated Line

Line 7-8 of Figure 3.1 is provided with 70% fixed series compensation and for simulating the condition of current inversion, line 5-7 is removed from the network shown in Figure 3.1 and Gen-2's source impedance is reduced. After these modifications are made in the system, A Lg fault is created in phase-a of line 7-8 at a distance of 30 km from bus 7 with fault resistance of 75 Ω at 1 s. Selected Features are given as input to the FLS. For relay close to bus 7 on line 7-8, first and second feature belongs to the set EZ, third, forth and fifth feature belongs to the set SN. For relay close to bus 8 on line 7-8, first and second feature belongs to the set EZ, third, forth and fifth feature belongs to the set SP. Variation of these features for both ends of line 7-8 is shown in Figure 5.17 and 5.18.

Output decision for line 7-8 and 8-7 are as shown in Figure 5.19. It shows that FLS

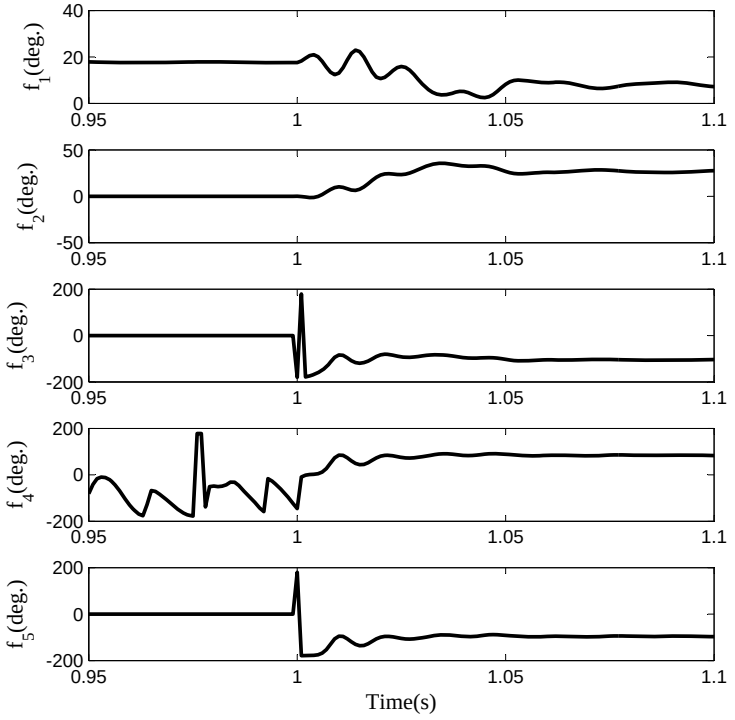

FIGURE 5.17: Variation of selected features at terminal of line 7-8 close to bus 7 for Lg fault on compensated line

has given output as "1" for both ends of line 7-8 and output as "0" for both ends of line 8-9. So based on fault element identification criteria given in 5.3, line 7-8 is correctly declared as faulted line.

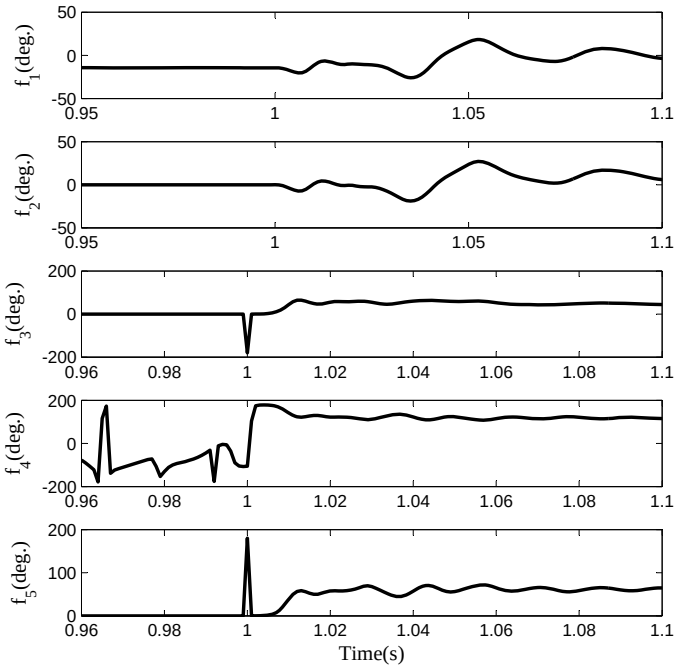

FIGURE 5.18: Variation of selected features at terminal of line 7-8 close to bus 8 for Lg fault on compensated line

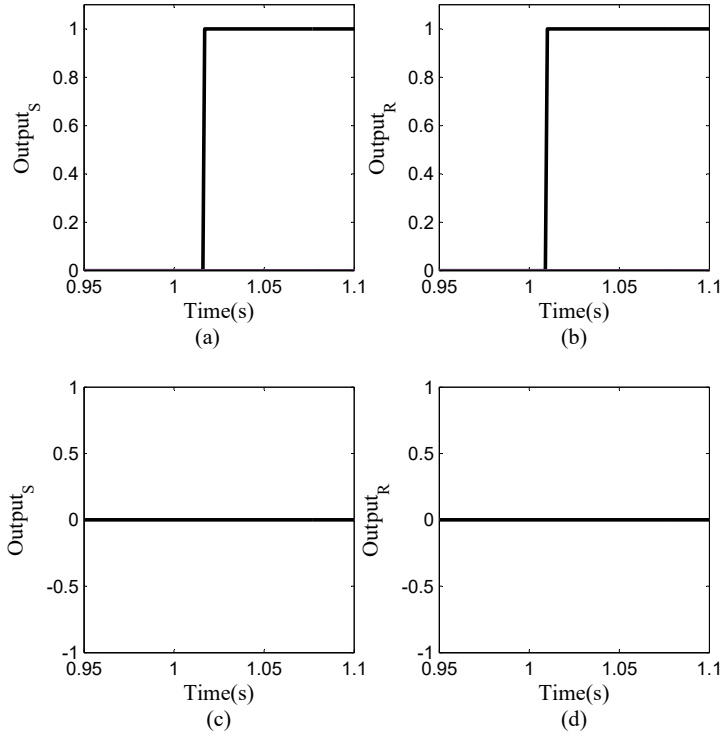

FIGURE 5.19: Performance for current inversion (a) and (b)Line 7-8, (c) and (d) Line 8-9.

5.3.5 Results for Three Phase Fault on Series Compensated Line

To analyze the performance of proposed method for voltage inversion, a 3 ϕ fault is simulated in line 7-8 at a distance of 60 km from bus 7 at 1 s. Selected Features are given as input to the FLS for determining the faulted line. For relay close to bus 7 on line 7-8, first feature belongs to SP, second feature belongs to EZ set, third feature belongs to the set SN. For relay close to bus 8 on line 7-8, first and second feature belongs to the set SP, third feature belongs to the set EZ. Variation of these features for both ends of line 7-8 is shown in Figure 5.20 and 5.21.

Output decision for line 7-8 and 8-7 are as shown in Figure 5.22. It shows that FLS

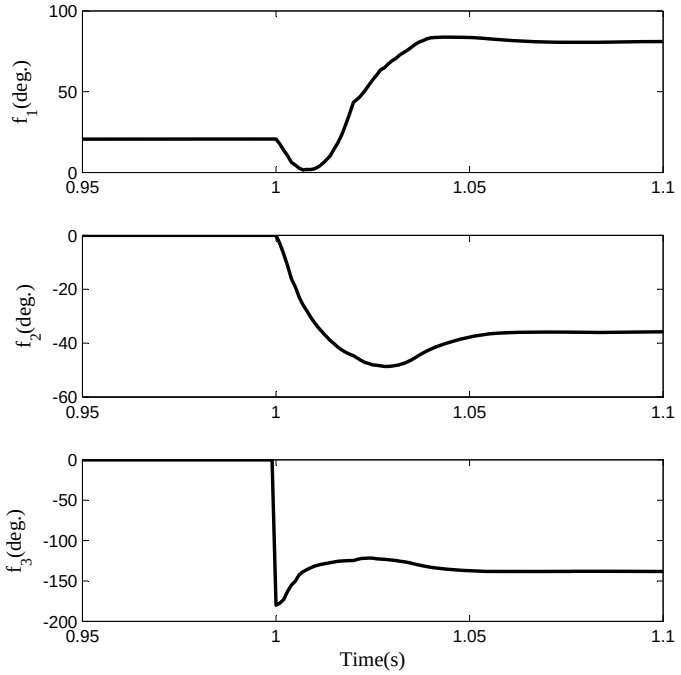

FIGURE 5.20: Variation of selected features at terminal of line 7-8 close to bus 7 for 3 ϕ fault on compensated line

has given output as "1" for both ends of line 7-8 and output as "0" for both ends of line 8-9. So based on fault element identification criteria given in 5.3, line 7-8 is correctly declared as faulted line.

5.3.6 Results during Load Encroachment

To analyze the performance of proposed method during load encroachment, loading of the bus 8 is increased at 1 s. Selected Features are given as input to the FLS. For relay close to bus 7 on line 7-8, first feature belongs to EZ, second feature belongs to EZ set,

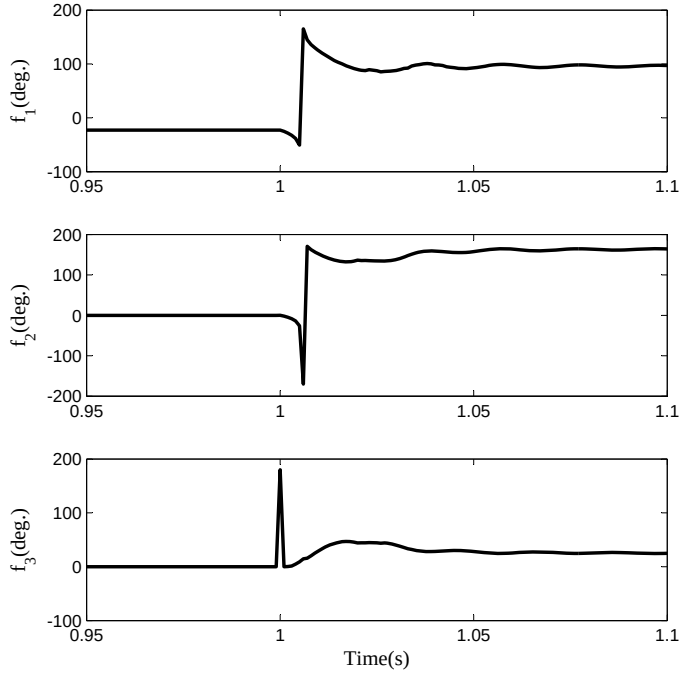

FIGURE 5.21: Variation of selected features at terminal of line 7-8 close to bus 8 for 3 ϕ fault on compensated line

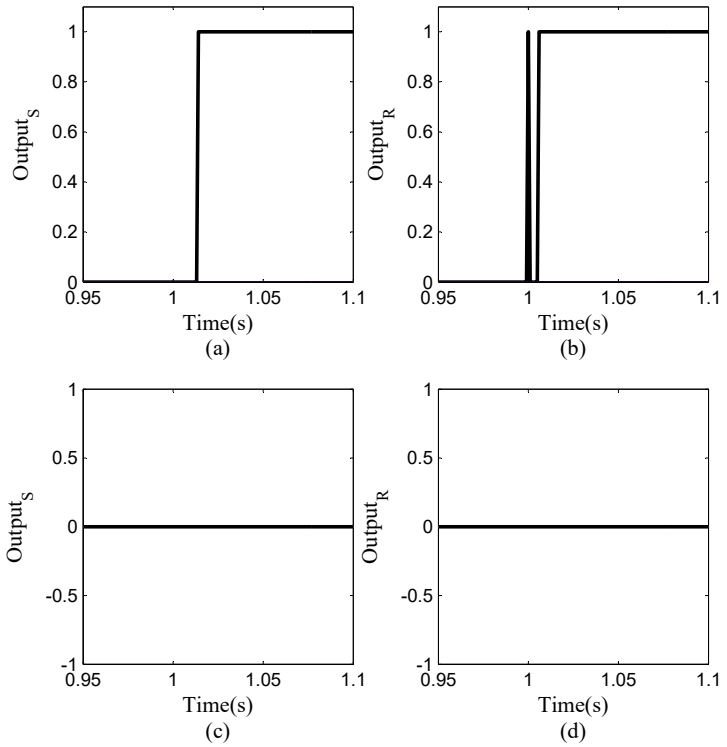

FIGURE 5.22: Performance for voltage inversion (a) and (b) Line 7-8, (c) and (d) Line 8-9.

third feature belongs to the set LN. For relay close to bus 8 on line 7-8, first and second feature belongs to the set EZ, third feature belongs to the set LN. Variation of these

features for both ends of line 7-8 is shown in Figure 5.23 and 5.24.

Output decision for line 7-8 and 8-7 are as shown in Figure 5.25. It shows that FLS

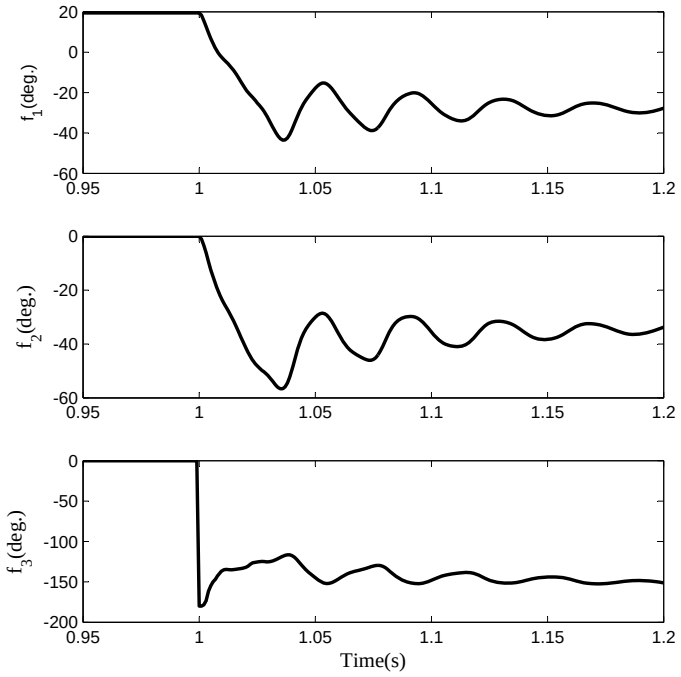

FIGURE 5.23: Variation of selected features at terminal of line 7-8 close to bus 7 during load encroachment

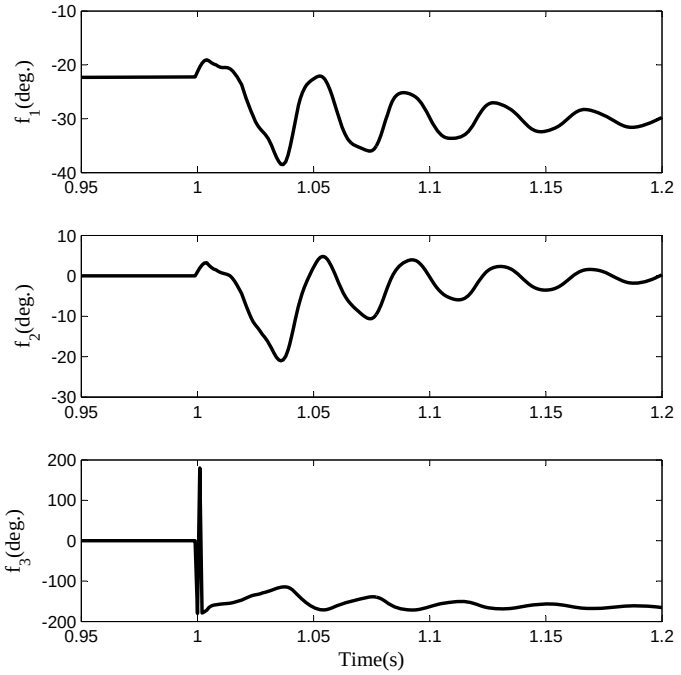

FIGURE 5.24: Variation of selected features at terminal of line 7-8 close to bus 8 during load encroachment

has given output as "0" for both ends of line 7-8 and output as "0" for both ends of line

8-9. So based on fault element identification criteria given in 5.3, no fault is detected in the system.

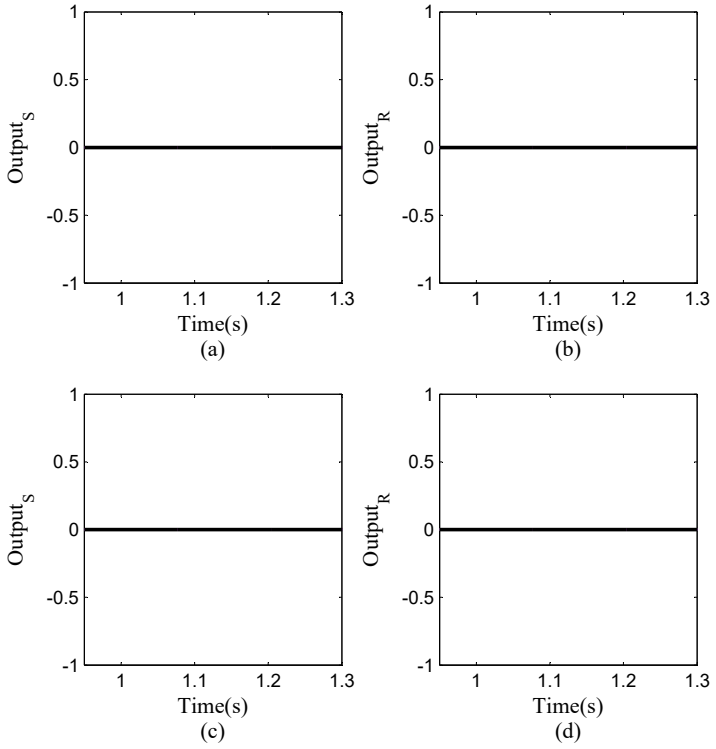

FIGURE 5.25: Performance for load encroachment (a) and (b) Line 7-8, (c) and (d) Line 8-9.

Chapter 6

Conclusion

WAMS technology is gaining popularity across the globe and numerous PMU installation projects are under implementation. One of the applications of WAMS technology for power system is in strengthening the performance of existing protection system. WAMS based protection techniques can help us to avert possible power system blackouts caused due to drawbacks in conventional protection systems. A PMU data based protection scheme for series compensated lines has been proposed in this thesis. Fuzzy logic system has been used for integrating useful information about selected features obtained by various sequence components. Critical issues in series compensated line protection such as current/voltage inversion have been successfully addressed by the proposed method. It is difficult to identify fault inception during power swing condition. Conventional fault detection scheme find limitation during power swing condition because of modulations in current and voltage waveform. A PMU data based protection scheme dedicated for fault detection during power swing has been presented. Firstly, inception of fault is identified by superimposed positive sequence power. After fault identification, faulted section is identified by using two different criteria for balanced and unbalanced faults. Performance of this method is tested for compensated and uncompensated lines.

6.1 Future Work

1. Performance of proposed methods can be further validated by performing hardware test.

2. With increasing application of FACTS devices in power transmission lines, a protection scheme using WAMS can be studied for application in these lines.

3. This work assumes that PMUs are available at all the buses. However, to reduce the economy of projects for protection of 220 kV and 132 kV voltage levels lines optimal PMU placement algorithm based protection scheme can be developed.

Bibliography

[1] S. H. Horowitz and A. G. Phadke, "Third zone revisited," *IEEE Trans. Power Del.,* vol. 21, no. 1, pp. 23-29, Jan. 2006.

[2] J. D. Ree, V. Centeno, J. S. Thorp, and A. G. Phadke, "Synchronized phasor measurement applications in power systems," *IEEE Trans. Smart Grid,* vol. 1, no. 1, pp. 20-27, Jun. 2010.

[3] A. Bose, "Models and techniques for the reliability analysis of the smart grid," in *Proc. IEEE Power Energy Soc. Gen. Meet.,* Sep. 2010, pp. 1-5

[4] H. M. Xu, T. S. Bi, S. F. Huang, Q. X. Yang, "Study on wide area backup protection to prevent cascading trips caused by flow transferring," *IEEE Power Engineering Soc. Transmission and Distribution Conf. and Expo.,* Oct. 09-14, 2005, New Orleans, Louisiana, USA.

[5] M. M. Eissa, M. E. Masoud, and M.M.M. Elanwar, "A novel backup wide area protection technique for power transmission grids using phasor measurement unit," *IEEE Trans. Power Del.,* vol. 25, no. 1, pp. 270-278, Jan. 2010.

[6] P. V. Navalkar and S. A. Soman, "Secure remote backup protection of transmission lines using synchrophasors," *IEEE Trans. Power Del.,* vol. 26, no. 1, pp. 87-96, Jan. 2011.

[7] J. Ma, J. Li, J. S. Thorp, A. J. Arana, Q. Yang, and A. G. Phadke, "A fault steady state component-based wide area backup protection algorithm," *IEEE Trans. Smart Grid.,* vol. 2, no. 3, pp. 468-475, Sep. 2011.

[8] Z. He, Z. Zhang, W. Chen, O. P. Malik and X. Yin, "Wide-area backup protection algorithm based on fault component voltage distribution," *IEEE Trans. Power Del.,* vol. 26, no. 4, pp. 2752-2760, Oct. 2011.

[9] M. Kalantar Neyestanaki and A. M. Ranjbar, "An Adaptive PMU-Based Wide Area Backup Protection Scheme for Power Transmission Lines," *IEEE Trans. Smart Grid.,* vol. 6, no. 3, pp. 1550-1559, May 2015.

[10] J. C. Tan, P. A. Crossley, P. G. McLaren, P. F. Gale, I. Hall, and J. Farrell, "Application of a wide area back-up protection expert system to prevent cascading outages," *in Proc. IEEE Power Eng. Soc. Summer Meeting,* 2001, vol. 2, pp. 903-908.

[11] S. Garlapati, H. Lin, A. Heier, S. K. Shukla, and J. Thorp, "A hierarchically distributed non-intrusive agent aided distance relaying protection scheme to supervise zone 3," *Int. J. Elect. Power Energy Syst.,* vol. 50, pp. 42-49, Sep. 2013.

[12] Yi Lv, Dahai You, Ke Wang, Liang Wang, Zhenhai Chen, Simin Huo, "Study on wide-area backup protection system for the smart grid," *IEEE, Electric Utility Deregulation and Restructuring and Power Technologies (DRPT),* July 2011, pp. 218-224, ISBN: 978-1-4577-0364-5.

[13] Zhenxing Li, Xianggen Yin, Zhe Zhang, and Zhiqin He, "Wide-Area Protection Fault Identification Algorithm Based on Multi-Information Fusion," *IEEE Trans. Power Del.,* vol. 28, no. 3, pp. 1348-1355, Jul 2013.

[14] P. K. Nayak, A. K. Pradhan, and P. Bajpai, "Wide-area measurementbased back-up protection for power network with series compensation," *IEEE Trans. Power Del.,* vol. 29, no. 4, pp. 1970-1977, Aug. 2014.

[15] A. G. Phadke, "The wide world of wide- area measurement," *IEEE Power Energy Magazine,* vol. 6, No. 5, pp. 52-65, October 2008.

[16] A. G. Phadke and J. S. Thorp. Synchronized Phasor Measurements and Their Applications. New York: Springer, 2008 ISBN 978-0-387-76535-8.

[17] *IEEE Standard for Synchrophasors for Power Systems,* IEEE Standard 1344-1995, December 1995.

[18] *IEEE Standard for Synchrophasors for Power Systems,* IEEE Standard C37.118-2005 (Revision of IEEE Std 1344-1995), March 2006.

[19] *IEEE Standard for Synchrophasor Data Transfer for Power Systems,* IEEE Standard C37.118.2-2011 (Revision of IEEE Std C37.118-2005), December 2011.

[20] *IEEE Standard for Synchrophasor Measurements for Power Systems,* IEEE Standard C37.118.1-2011 (Revision of IEEE Std C37.118-2005), December 2011.

[21] *IEEE Guide for Phasor Data Concentrator Requirements for Power System Protection, Control, and Monitoring,* IEEE Standard C37.244-2013.

[22] B. Kasztenny, "Distance protection of series-compensated lines: problems and solutions," presented at the *28th Annu. Western Protect. Relay Conf.,* Spokane, WA, USA, Oct. 22-25, 2001.

[23] D. Novosel, A. G. Phadke, M. M. Saha, and S. Lindahl, "Problems and solutions for microprocessor protection of series compensated lines," *in Proc. Conf. Develop. Power Syst. Protect.,* 1997, pp. 18-23.

[24] A. Y. Abdelaziz, A. M. Ibrahim, M. M. Mansour and H. E. Talaat, "Modern approaches for protection of series compensated transmission lines," *Elect. Power Syst. Res.,* vol. 75, pp. 85-98, 2005.

[25] R. J. Marttila, "Performance of distance relay mho elements on MOV protected series-compensated lines," *IEEE Trans. Power Del.,* vol. 7, no. 3, pp. 1167-1178, Jul. 1992.

[26] P. K. Nayak, A. K. Pradhan and P. Bajpai, "A fault detection technique for the series-compensated line during power swing," *IEEE Trans. Power Del.,* vol. 28, no. 2, pp. 714-722, Apr. 2013.

[27] P. Jena and A. K. Pradhan, "A positive-sequence directional relaying algorithm for series-compensated line," *IEEE Trans. Power Del.,* vol. 25, no. 4, pp. 2288-2298, Oct. 2010.

[28] P. Jena and A. K. Pradhan, "Directional Relaying in the Presence of a Thyristor-Controlled Series Capacitor," *IEEE Trans. Power Del.,* vol. 28, no. 2, pp. 628-636, Apr. 2013.

[29] D. L. Goldsworthy, "A linearized model for MOV-protected series capacitors," *IEEE Trans. Power Syst.,* vol. PWRS-2, no. 4, pp. 953-957, Nov. 1987.

[30] Z. D. Gao and G. B. Wang, "A new power swing block in distance protection based on a microcomputer-principle and performance analysis," *in Proc. Int. Conf. Adv. Power Syst. Control, Oper. Manage.,* Hong Kong, China, Nov. 1991, vol. 2, pp. 843-847.

[31] G. Benmouyal, D. Hou and D. Tziouvaras, "Zero-setting power-swing blocking protection," *presented at the the 31st Annual Western Protective Relay Conf.,* Spokane, WA, Oct. 2004.

[32] A. P. Apostolov, D. Tholomier, and S. H. Richards, "Superimposed components based sub-cycle protection of transmission lines," *in Proc. IEEE Power Eng. Soc. Power Syst. Conf. Expo,* Oct. 2004, vol. 1, pp. 592-597.

[33] M. M. Eissa, "Evaluation of a new current directional protection technique using field data," *IEEE Trans. Power Del.,* vol. 20, no. 2, pp. 566-572, Apr. 2005.

[34] J. G. Rao and A. K. Pradhan,"Application of synchrophasor data for fault detection during power swing," *Energy, Automation, and Signal (ICEAS), 2011 International Conference,* Bhubaneswar, Odisha, 2011, pp. 1-5.

[35] P. G. McLaren, G. W. Swift, Z. Zhang, E. Dirks, R. P. Jayasinghe, and I. Fernando, "A new directional element for numerical distance relays," *IEEE Trans. Power Del.,* vol. 10, no. 2, pp. 666-675, Apr. 1995.

[36] P. Jena and A. K. Pradhan, "An integrated approach for directional relaying of double circuit line," *IEEE Trans. Power Del.,* vol. 26, no. 3, pp. 1783-1792, Jul. 2011.

Appendix

System data for modified WSCC 9 bus system used for the simulation.

Generator Data

Gen 1: 600 MVA, 22 kV, 50 Hz, inertia constant = 4.4 MW/MVA.
$X_d = 1.81$ p.u., $X_d^{'} = 0.3$ p.u., $X_d^{''} = 0.23$ p.u., $T_{do}^{'} = 8$ s, $T_{do}^{''} = 0.03$ s, $X_q = 1.76$ p.u.,
$X_q^{''} = 0.25$ p.u., $T_{qo}^{''} = 0.03$ s, $R_a = 0.003$ p.u., $X_p = 0.15$ p.u.
Gen 2: 465 MVA, 22 kV, 50 Hz
Gen 3: 310 MVA, 22 kV, 50 Hz

Transformer Data

T1: 600 MVA, 22 kV, 50 Hz, Δ / Y
X = 0.163 p.u., $X_{core} = 0.33$ p.u., $R_{core} = 0.0$ p.u., $P_{copper} = 0.00177$ p.u.
T2: 465 MVA, 22 kV, 50 Hz, Δ / Y
T3: 310 MVA, 22 kV, 50 Hz, Δ / Y

Transmission Line Data

Positive sequence impedance = 0.03293 + j0.327 Ω/km
Positive sequence capacitive reactance = 280.1 x 103 Ω*km
Zero sequence impedance = 0.2587 + j1.174 Ω/km
Zero sequence capacitive reactance = 461.2546 x 103 Ω*km
Line 7-8 is 70% series compensated.

Transmission Lines Length

Line 7-8: 320 km

Line 8-9: 400 km

Line 9-6: 300 km

Line 6-4: 350 km

Line 4-5: 350 km

Line 5-7: 310 km

Loads

Load A = 300 MW + j100 MVAR

Load B = 200 MW + j75 MVAR

Load C = 150 MW + j75 MVAR